ISSN 2347-3487

In situ measurement shows ocean boundary layer physical processes control catastrophic global warming.

J. Brian Matthews and J. B. Robin Matthews
Drs J B and J B R Matthews, Douglas, Isle of Man, British Isles
drs-matthews@manx.net
Dept of Physics and Physical Oceanography, Memorial University of Newfoundland, St Johns, NL, Canada

ABSTRACT

The infrared greenhouse gas heat trap at the top of the atmosphere controls anthropogenic global warming (AGW) heat balance. Processes at the top of the ocean similarly control the 93% of AGW in the oceans. The tropics are a global year-round ocean heat source. Heat is transported in the ocean by sinking brine from tropical evaporation and polar freezing. Buoyant freshwater and ice barriers limit heat loss from the surface layer. The almost completely unstudied ocean surface skin is critically important to understanding global warming and climate change processes. Studies to date have concentrated on atmospheric warming mainly from land-air data. In this paper we present the first hourly meridional 3m and surface observations in the equatorial Pacific from Tahiti to Hawaii for direct measurement of evaporation and ocean boundary layer heat trapping. We relate this to poleward heat and freshwater transport and ocean warming moderation by basal icemelt of floating ice explored in a second paper [1].

We show heat sequestration below 3m in the hypersaline (>35.5‰) southern hemisphere (SH) is limited to ~6MJm^{-2}day^{-1} but evaporation is 7.3mm m^{-2}day^{-1}, at salinity ~36.4‰ and temperature >28°C. In the northern hemisphere (NH) tropics the corresponding figures are ~12 MJm^{-2}day^{-1} and ~4.5mm m^{-2}day^{-1}. Equatorial upwelling and the 50m deep Bering Strait limit buoyant surface outflow from the North Pacific.

We found pairs of counter-rotating vertical meridional tropical cells (MTCs), ~300-1200km wide, ~100m deep form separate SH and NH systems with little cross-equatorial flux. Counter-rotating Lagrangian wind-driven gyres transport heat and freshwater polewards in seasonally and tidally moderated stratified surface waters. The zonal geostrophic balance is maintained by the Equatorial Undercurrent (EUC) with an eastbound core ~140cms^{-1} and density ~25.0 at 50-150m.

Global warming and polar icemelt has been underestimated from wrong assumptions of the processes in the top 3m of oceans. These are the unverified beliefs that ocean evaporation depends on windspeed and relative humidity that the ocean is well mixed to 10m depths, and by neglect of water density determined by both salinity and temperature. Temperature measurement to ±0.01°C is required to account for the 3000x greater volumetric heat capacity of seawater to air (3.9x10^{6}: 1.3x10^{3}Jm^{-3}°C^{-1}). Most SST data are to atmospheric standards (>±0.5°C). Evaporation depends only on temperature (Clausius-Clapeyron). Heat sequestration depends on the buoyant surface layer processes and underlying density gradient. Eleven interconnected counter-rotating Lagrangian wind-driven surface gyres form a global circulation system that carries buoyant surface water masses at speeds much higher than Eulerian geostrophic currents. Polar ice may erode year-round from basal melting from warm subsurface water.

This explains contrasting Arctic/Antarctic warming impacts. We suggest many more in situ 3m timeseries especially meridional ones are needed to confirm our findings. In a second paper on centennial daily surface timeseries we show ocean surface warming trend rate post about 1976-1986 is ~0.037ºCyr^{-1}, i.e. >1ºC in 20 years [1]. We suggest global warming research be concentrated on the top of the ocean through multidisciplinary timeseries fieldwork verification, monitoring and modeling. This would best be conducted through a cost-efficient dynamic adaptive scientific management for rapid determination of mitigation and adaptation strategies. Reducing troposphere greenhouse gases can only reduce warming. Mitigation maybe possible through heat energy extraction from geothermal, ocean, tidal and solar sources.

ISSN 2347-3487

Indexing terms/Keywords

1986 rapid warming trend, 250-year global heat balance, Age of seawater, Ageostrophic current, Air-sea interaction, air-water specific heat, Aleut gyre, Alpha/beta global circulation, Anthropogenic global warming (AGW), Anticlockwise-clockwise gyres, Arafura Sea, Araruama hypersaline lagoon, Arctic brine, asymmetric climate change, asymmetric equatorial evaporation, asymmetric heat trap, asymmetric Pacific warming, Asymmetric sea surface density, asymmetric sea surface salinity, asymmetric sea surface temperature, asymmetric seawater latent heats, Atacama Desert, Atlantic Decadal Oscillation (PDO), Atlantic equatorial upwelling, basal polar icemelt, Beaufort gyre, Beaufort Scale super typhoon extension, Benguela current, Bering Strait, Brackish water, brine formation, brine from evaporation, brine from freezing, Bucket temperature, Buoyant surface water, carbon dioxide concentration, carbon dioxide heat trap, Carmack freshwater circulation, catastrophic global warming, Centennial cycles, Clausius-Clapeyron evaporation, Cold tongue equatorial water, Columbus gyre, Counter-rotating cells, Counter-rotating gyres, Current shear, Cyclonic-anticyclonic gyres, Daily timeseries, Decadal cycles, Density current, Density flux, Density gradient, Density gradient meridional, Density gradient vertical, Diurnal heat flux, Diurnal salinity variation, Diurnal salt flux, Diurnal temperature variation, Double diffusion, Down-welling rate, Drift currents, Drifter model OSCURS, Drifters Planktonic, Drifters sail-area, Drifters self-propelled, Drifters surface, Ebbesmeyer gyres, Eddy diffusion measurement, Eddy viscosity, Ekman current, El Niño/Southern Oscillation (ENSO), Energy balance, Engine room warming, Equatorial undercurrent (EUC), equatorial upwelling, Estuarine circulation, Estuary definition, Estuary stratification-current shear, Evaporation, Evaporation in situ measurement, Evaporation not-relative-humidity-dependent, Evaporation not-windspeed-dependant, Evaporation ocean, Evaporation rate, Evaporation temperature dependence, Evaporative cooling, Evaporative heat capture, Evaporative heat loss, Extreme weather, Flood enhancement, Flotsam drift, flotsametrics, Flux of freshwater, Fossil fuel heat trap, Freshwater flux, Freshwater freezing, Freshwater heat trap, freshwater transport, Fronts ocean, Garbage patches, Geophysical timeseries, Geostrophic current, GISS SST datasets, Global energy balance, global scale estuary, Global sea surface circulation, global warming, Great Barrier Reef tropical shelf sea, Gulf Stream, Gyre convergent/divergent, Gyre name, Gyre period, Gyre speed, Gyres counter-rotating, Hadley Cells, Hadley Centre SST datasets, Halocline, Heat diffusion coefficient, Heat imbalance, heat transport, Heyerdahl gyre, Hourly timeseries, Human induced warming, Humboldt current, Hurricane growth/decay, Hurricane heat extraction, hypersaline evaporation, hypersaline Great Barrier Reef Shelf Sea, Indian Ocean equatorial upwelling, IPCC post-2014, Isohaline, Isopycnals, Isothermal, Jet streams ocean, Lagrangian gyres, Lagrangian ocean circulation, Latent heat seawater, log of carbon dioxide concentration, Logarithmic surface wind drift, Majid gyre, Maunder minimum, Maverick science, Melville gyre, Meridional overturning circulation, Meridional tropical l cells (MTC), Millennial cycles, misuse of models, misuse of surface physics, Mitigation of ocean warming, Mixed layer theory, Multidiscipline adaptive research management, Navigator gyre, Near-surface salinity, Non-scientist data collection, North Atlantic Front, North Equatorial Current (NEC), North Pacific Front, Ocean acidification, ocean evaporation measurement, Ocean garbage patches, ocean global estuary, ocean heat capture, Ocean heat content, Ocean heat evaporation density-dependence, ocean surface circulation, ocean surface dynamics, Ocean surface gyres, Ocean surface physics, ocean surface thermodynamics, ocean warming, Oceanographic data processing, Pacific Decadal Oscillation (PDO , Pacific global scale estuary, Pacific Ocean equatorial upwelling, Panama Isthmus, Penguin gyre, polar amplification, Polar Bear gyre, Polar brine formation, Precipitation flooding sealevel change, Precipitation hypersaline-enhanced, Precipitation induced sealevel change, Pycnocline, radiation forcing Human-induced, Radiation forcing natural, Radiation forcing solar/sunspot, Relative humidity , Salinity gradient meridional, Salinity gradient vertical, Salt diffusion, Satellite sea surface temperature, scientific method field verification, Sea ice heat trap, Sea surface density, Sea surface evaporation, Sea surface Lagrangian circulation, Sea surface salinity (SSS), Sea surface temperature (SST), Seawater evaporation, Seawater freezing, Shelf seas, Solar radiation climate change, South Equatorial Current (SEC), Specific heat seawater, SST dataset errors, Storkerson gyre, Stratification, Sunspot cycle, Sunspot ocean decadal cycles, super typhoon, Surface currents, Surface density, Surface drifters, Surface residence duration, Surface salinity, Surface temperature, Tahiti-Hawaii, Tahiti-Hawaii, Thermal diffusion coefficient, Thermocline, Thermosalinograph, Top of ocean

heat trap, Top of ocean heat trap, Torres Strait, Tropical brine , Tropical brine , tropical evaporation, tropical evaporation, Tropical meridional cells, TS diagram, TS-Evaporation diagram, Turtle Gyre, Turtle Gyre, Twentieth Century sunspot maximum, Unstoppable global warming, Unstoppable global warming, Unstudied top-of-ocean, Upwelling rate, Verification fieldwork, Vertical mass diffusion, vertical meridional tropical cells (MTCs), vertical meridional tropical cells (MTCs), Viking gyre, Viking gyre, Walker Cells, Water mass fronts, Western warm boundary current, Wind-driven currents, Windspeed evaporation

Academic Discipline And Sub-Disciplines

Physics of top of ocean, in situ experimental data, timeseries, global warming

SUBJECT CLASSIFICATION

Physical oceanography

TYPE (METHOD/APPROACH)

Experimental fieldwork, analysis and review

ISSN 2347-3487

1 INTRODUCTION

The infrared greenhouse gas heat trap at the top of the atmosphere controls anthropogenic global warming (AGW) heat balance. Processes at the top of the ocean similarly control the 93% of AGW in the oceans. The tropics are a global year-round ocean heat source. Heat is transported in the ocean by sinking brine from tropical evaporation and polar freezing. Buoyant freshwater and ice barriers limit heat loss from the surface layer. The almost completely unstudied ocean surface skin is critically important to understanding global warming and climate change processes. Studies to date have concentrated on atmospheric warming mainly from land-air data. In this paper we present the first hourly meridional 3m and surface observations in the equatorial Pacific from Tahiti to Hawaii for direct measurement of evaporation and ocean boundary layer heat trapping. We relate this to poleward heat and freshwater transport and ocean warming moderation by basal icemelt of floating ice explored in a second paper [1].

1.1 Top of Atmosphere and top of ocean anthropogenic greenhouse gas warming

The top-of-the-atmosphere greenhouse gas heat trap resulting in a net energy imbalance lies over the ~9-16km deep atmosphere. It comprises mainly carbon dioxide because water vapor is not present in the troposphere. This forms the outer heat trap barrier controlling Earth's energy balance. The ~200m deep top-of-the-ocean heat trap barrier lies over -4.5km deep oceans that includes the 8.5% of the ocean surface in the <200m deep shelf seas (Figure 1).

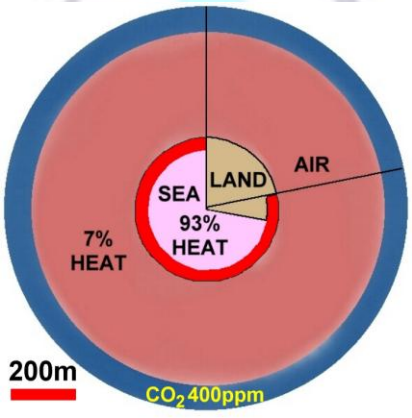

Figure 1 Global anthropogenic heat trap at top of atmosphere and top of ocean

The ocean surface skin controls ocean heat imbalance, evaporation and radiative heat balance. Surface bucket or bulk temperatures in the upper 0.5-1m measured surface heat. Satellite skin temperatures are calibrated to surface bucket bulk temperatures. Sinking brine from evaporation in the tropics and freezing in Polar Regions transports heat into the oceans. Seawater density depends on temperature and salinity. Therefore, surface salinity is important to ocean heat capture but data a very rare.

From 1955-2010 the increase in global ocean heat content is estimated to account for 93% of observed anthropogenic warming with largest part in the upper tropical Pacific [2]. A physics-based re-analysis and verification of land-air records from 1753-2011 showed a global temperature increase of 1.5°C in the past 250y and 0.90±0.05°C in the past 50y [3]. All observed land-air warming could be modeled solely from the sum of volcanism and a single anthropogenic proxy (log of CO_2 concentration) without a contribution from solar forcing. The present CO_2 concentration of 400ppm is therefore 6.3% greater than the 400kyr stable heat balance mean of 280ppm. The model correctly replicates all features of observed land-air temperatures including multi-decadal and internal temperature changes. The only exception was at the peak of the mid-twentieth century sunspot cycle in the 400yr since the Maunder Minimum [1]. Peak irradiation, two standard deviations above long-term means, led to record warm air and water and, 3½ years later, record cold winter from Arctic basal icemelt

ISSN 2347-3487

However, the suggested 'missing heat' is not understood [4]. Recent comparison of modern ocean temperatures to the Challenger (1872-1876) datasets suggests the net top-of-the-atmosphere energy imbalance 1873-1955 was 0.1±0.06 W m^{-2} [5]. Further comparison with the Challenger datasets suggests mean global ocean temperatures increased by 0.59±0.12°C at the surface, by 0.39±0.18°C below 366m (200 fathoms) and by 0.12±0.07°C at 914m (500 fathoms) [6]. This suggests centennial timescales for ocean warming.

Temperature timeseries data in the upper 50m is sparse especially in the equatorial Pacific. Near-surface salinity data in the upper 10m is not available. Therefore equatorial heat balance computations are based on sea surface temperature (SST) averaged over the upper 100m [2]. Since temperature is a massless quantity and ocean heat is transported by the water mass, ocean heat calculations based on SST are not a reliable indicator [7].

We developed this work to study discrepancies between Hadley Centre and GISS SST datasets [8-9]). It was thought discrepancies arose from mid-twentieth century changes to SST measurement methods from buckets to engine room intake water to satellite temperatures. We designed the experiment to compare hourly bucket temperatures from three different bucket types, 3m-depth scientific water intake thermosalinograph (TSG), standard meteorological, and daily CTD data. Later, corresponding satellite skin temperatures for nearby satellite footprints were added. These are routinely corrected to bulk bucket temperatures (Figure 2).

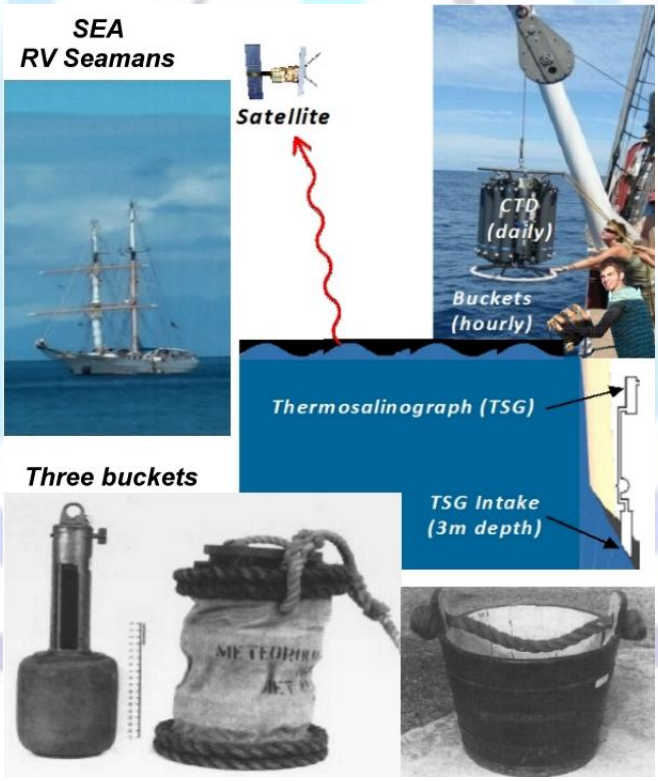

Figure 2 Central tropical Pacific surface hourly timeseries experiment between Tahiti and Hawaii 17°S-22°N, 140-150°W May-June 2008.

We found engine intake data from unknown depths were the most likely error source. Corrections for evaporative cooling were invalid in light of the short sampling time and large heat capacity of a bucket of water. We suggested database errors be removed [9]. It is important they be corrected because SST datasets are widely used for climate modelling, ocean heat balance, long-term climate change, ocean acidification and ecological studies among others. It is standard data processing procedure to alter raw SST data from 20th century for unverified corrections for evaporative bucket cooling and engine room warming [10]. A corrected SST ocean climate dataset has been constructed and applied in an attempt to understand surface carbonate chemistry and ocean acidification [11]. However, invalid data remain SST datasets.

ISSN 2347-3487

1.2 Pacific Ocean equatorial SST timeseries

The adjustment for engine room warming of seawater intakes from unknown depths is particularly troubling given the persistent near-surface temperature gradients observed in all oceans [12]. The importance of the top few metres of ocean is clearly visible in our Pacific temperature timeseries (Figure 3). It shows hourly temperatures from dry air, the mean of three different bucket types, 3m thermosalinograph (TSG) 20m daily noon CTD [8]. This confirmed the expected wide daily range of air, surface and subsurface temperatures. The difference between surface buckets (red), 3m TSG (blue) and 20m CTD (yellow) temperatures are clearly visible (Figure 3). Surface buckets data were not collected beyond 3°N.

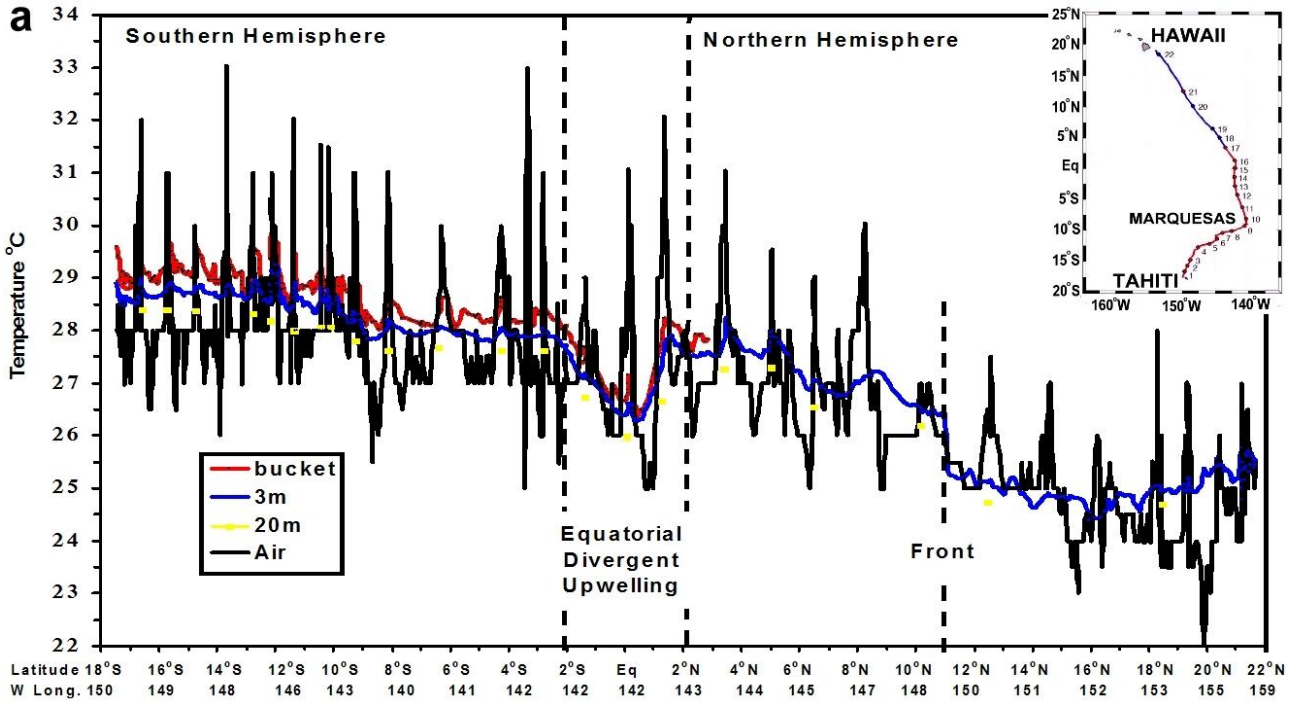

Figure 3) Meridional hourly temperatures for the mean of three different bucket types at the surface, 3m TSG, dry bulb air and 20m CTD. Inset cruise track RV Seamans 11 May – 12 June 2008 Tahiti-Marquesas-Hawaii.

At this timescale the concept of a single value sea surface temperature (SST) measured to about ±0.5ºC substituted for marine air temperature in atmospheric models becomes problematic. Mean sea surface temperatures are warmer than 3m temperatures that are themselves warmer than 10m dry air temperatures. Air temperatures show the widest diurnal variations because of the 3000x greater volumetric heat capacity of seawater to air ($3.9x10^6$: $1.3x10^3 Jm^{-3}°C^{-1}$).

Three distinct temperature regimes are visible in the record. The southern hemisphere warm regime is separated from the colder northern hemisphere by the cold equatorial divergent upwelling between 2°S and 2°N. The southern hemisphere has fairly uniform temperatures >28°C. The northern hemisphere is separated by a strong frontal system between two water masses at the about the density but with ~2°C temperature difference at about 11°N [1].

The daily mean temperature variation alerted us to the false assumption of a uniform top 10m ‘mixed layer’ of ocean widely used in climate studies. This assumption was used as the basis for substituting engine intake temperatures from unknown depth in lieu of bucket surface temperatures. Unsupervised, non-scientist observers collect much of these data on ships of opportunity sailing on commercial shipping routes [8-9]. Moreover, data from large tracts of ocean especially on mid-ocean meridional tracks are completely absent from datasets. Our meridional transect is valuable in highlighting the problem.

ISSN 2347-3487

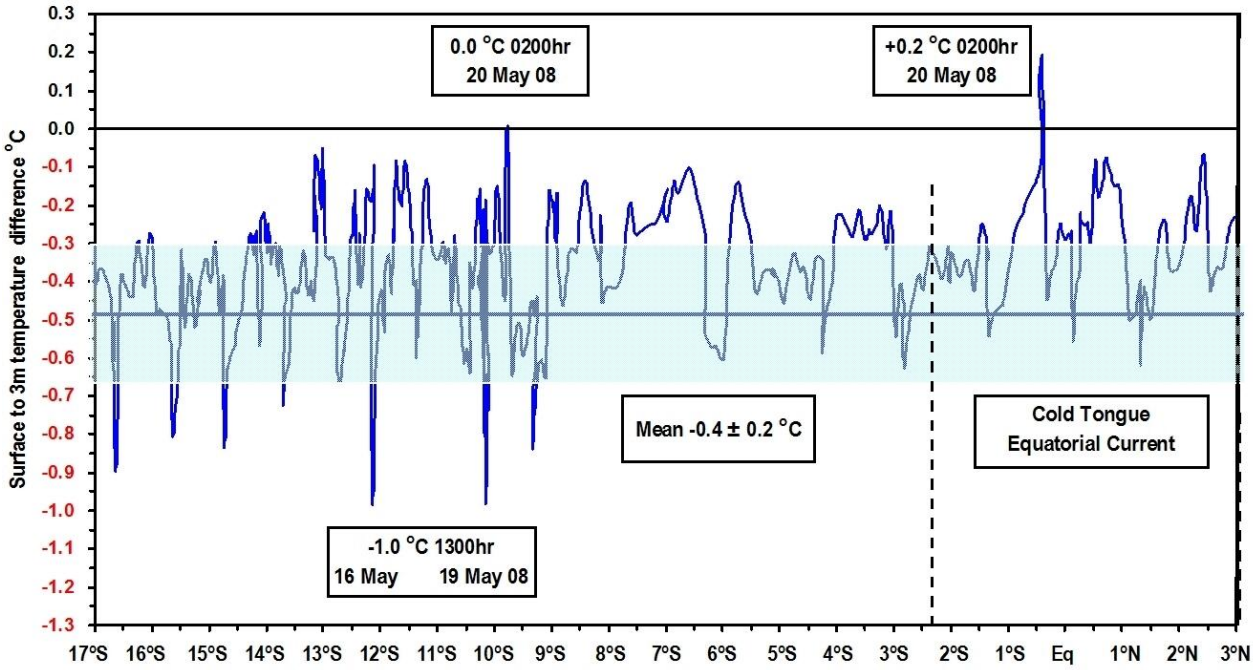

Figure 4) Surface to 3m temperature differences between 17°S-3°N

The daily mean temperature range over the top 3m of ocean was -0.4±0.2ºC (shaded light blue) (Figure 4) [9]. Temperatures decreased with depth as expected. The largest differences were –1.0ºC at 13:00LT at 12.1ºS and 10.1ºS. The smallest gradients were at late night with 0ºC at 10ºS at 02:00LT. There was a short temperature inversion of +0.2ºC at 0.4ºS over the divergent equatorial upwelling and cold tongue. So together with salinity at 3m we can determine surface heat penetration and evaporative brine production. This is focus of the present paper.

If engine room warming were real, it suggested that temperatures were biased warm by a few tenths of a degree. Then a temperature reduction would be applied. Temperature declines with depth so adjustment of raw data this way would exaggerate the decline. It is possible by using such unverified methods that significant climate shifts such as that reported by Crawford et al, [13] for the North Pacific from 1955-2005 could be removed from datasets. However, data for the upper 10m are not available though warming of similar or greater magnitude is likely (W. Crawford, personal communication).

1.3 Oceans as stratified estuaries

Thermal stratification observed in all oceans allows characterization of ocean surface processes as estuarine in nature. Estuaries are defined in terms of density stratification (temperature and salinity) and current shear [14]. As early as 1960 Tully and Barber suggested the sub-polar north Pacific was a classic stratified estuary with a surface brackish layer continuously renewed by relatively unvarying precipitation over a sub-Ekman ~135m halocline of salinity ~33.8‰ [15]. By 1984 the whole north Pacific was considered a global-scale estuary with limited stratified surface brackish outflow through the 50m Bering Strait into the Arctic Ocean Canada basin [16]. Carmack (2007) stated, “Climate change and climate-related impacts on essential industries (e.g. fisheries, agriculture, water resources) are not strictly about temperature, but also (perhaps mainly!) about the flux, distribution and phase of freshwater components in the atmosphere and ocean”. [17]. He described an alpha/beta salt/temperature dominated circulation of thermohaline stratified, low salinity, nutrient-rich surface waters as a downhill journey along pycnoclines from the stratified north Pacific, through 50m-deep Bering Strait and the highly-stratified Arctic Ocean, to the North Atlantic. It is an important part of global ocean circulation. We quantify the alpha/beta regimes.

ISSN 2347-3487

1.4 Lagrangian coherent surface gyre circulation

Lagrangian coherent water masses have only recently received attention although reported as early as 1954 [1,18-20]. We adopt the gyre nomenclature proposed by Ebbesmeyer and Scigliano [21] because they refer specifically to surface Lagrangian wind-driven/geostrophic gyres (Figure 5) [1]. Gyre speeds are in nautical miles per day (nautical mile = 1.85km).

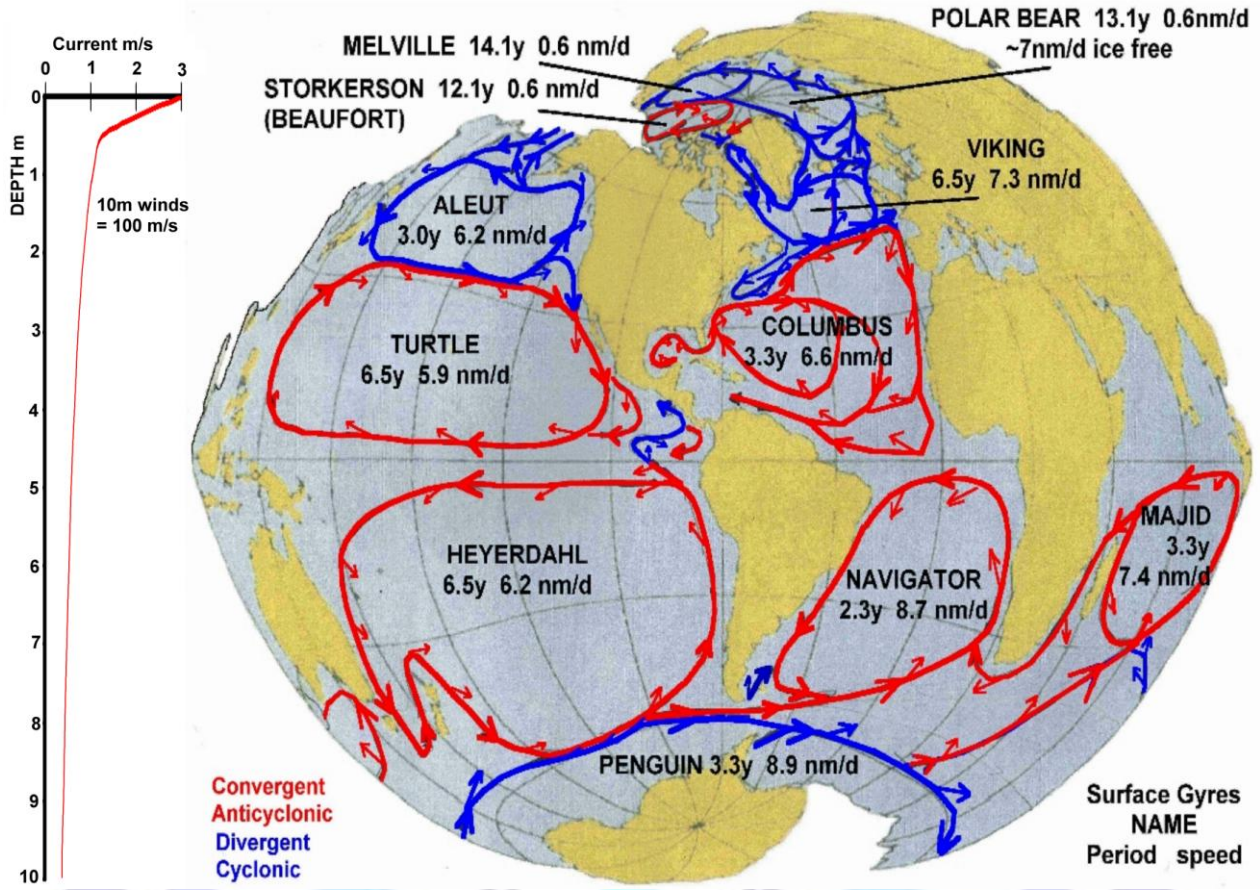

Figure 5 left) Logarithmic surface drift currents for 100 ms^{-1} winds, and Ebbesmeyer named interconnected counter-rotating divergent (blue)/convergent (red) Lagrangian surface gyres on an equal area projection.

The ocean surface obeys the log law of surface currents driven by winds that applies to oil spills, flotsam and surface drifters (Figure 5 left) [22]. Practically this means that surface drift is ~3% of windspeed and 3-4° to the right (left) in the northern (southern) hemisphere [23]. Drift is shown for winds of 100ms^{-1} at the standard 10m-anemometer height. Ekman spiral, exponentially decreasing currents dominate below the surface Lagrangian layer.

The gyre system has been confirmed from daily data 1902-1997 in the North Pacific with the OSCURS numerical model tuned to very extensive experimental Lagrangian surface drifter studies and daily geostrophic and surface wind data [21, 24--26]. Surface wind drift coefficients were verified for passive plankton-carrying watermasses and surface drifters, self-propelled drifters and those with appreciable sail areas that are enhanced by 30-50%. All oceans have garbage patches in convergent (red) surface gyres [27-30]. Our study area is a meridional transect across the westbound Turtle and Heyerdahl gyres 140-150°W.

2 METHODS

Data were processed in 24hr complete days and resolved into meridional components including surface, 3m TSG and atmospheric wet and dry bulb temperatures and TSG salinity and 10m winds. Ekman meridional and zonal ageostrophic

current computations were made from the 10m winds in the usual manner with the cold tongue wind stress drag coefficient $1.5x10^{-3}$ [31-32]. Density was computed from TSG data based on shallow water (<6km) approximations [33, 1].

3 RESULTS

The overall results of the temperature regime are shown in Figure 3 and briefly summarized here. There was an overall cooling northwards along the cruise track (>28 to <25ºC). Diurnal cycles are clear over continuous meridional mean daily travel of ~200km, ~1.3º latitude, through the cold equatorial tongue. Daily cruise tracks were longer in the NH than in the SH due to more intensive data collection in the SH [9]. The TSG record, accurate to ±0.01ºC, falls into three temperature regimes; 1) in the SH to the equatorial divergence zone, 2) the NH warm, and 3) the NH colder zone. The zones are separated by the equatorial divergent upwelling and cold tongue and a NH cold front region where temperatures fell 27.2-25.0ºC centered at ~11.1ºN. The cold front region temperature drop of 2.2ºC masked the diurnal temperature cycle as the vessel crossed during one complete day (5 June 2008). The abrupt 12.2km front with temperature drop of 1.1ºC was crossed at 11.1-11.2ºN [1]. Surface bucket or bulk temperatures from three different bucket types were measured to ±0.1ºC between 17.5ºS and 3ºN. The mean of three different bucket samples each hour is plotted. Differences clearly extended to at least 20m as shown by ~daily CTD temperatures. The persistent temperature gradient suggests continuous 24/7 wind-driven and thermohaline circulation (Figure 4).

3.1 Current depth profile

Meridional profile of E-W currents from 20-300m between 18ºS - 19ºN from an Acoustic Doppler Current Profiler (ADCP) is shown in Figure 6.

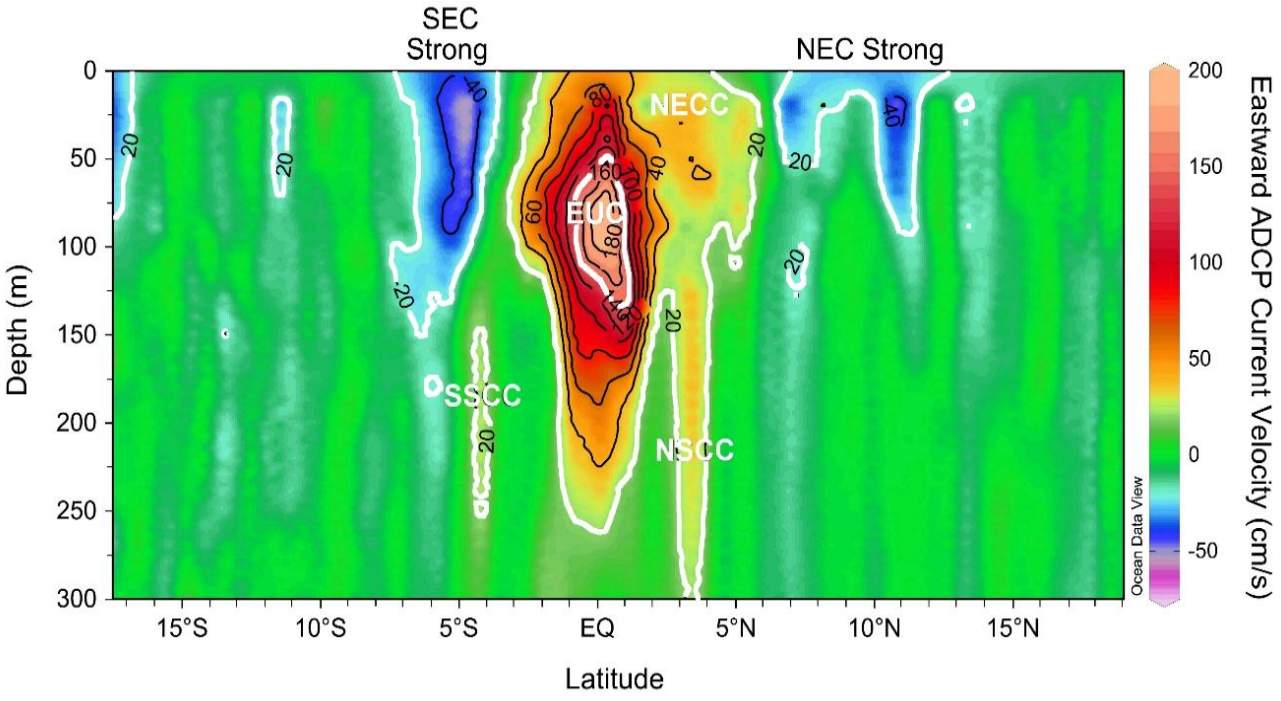

Figure 6 Subsurface current profiles of E-W currents from 20-300m between 18ºS - 19ºN from an Acoustic Doppler Current Profiler (ADCP)

Two westbound zonal currents >20cm/s were found, the South Equatorial Current (SEC) at ~9ºS and 2.5ºS, and the North Equatorial Current (NEC) at 6-11ºN and 12ºN. The subsurface eastbound Equatorial Undercurrent (EUC) >20cm/s with a core >140cm/s was at 50-150m. We note that the EUC is a vertically elongated annulus in section. The vertically elongated outer core maximum ~140cm/s has a lower ~80cm/s inner core. This is consistent with the EUC maintaining

geostrophic balance [34]. It has been reported as a 500km wide, ~200m deep core of salty warm water flowing ~14,000km from north of Papua New Guinea (~5ºS, 150ºE) to turn eastwards along the equator [35]. It transports water of eastwards decreasing density ~26.5-23.0 from SH western warm pool to upwell north of the equator in the eastern Pacific warm pool and beyond [36]. At 140ºW EUC lies within ±3º of equator, is 90% SH origin and shows seasonal variation. Fresh or brackish waters overlie both east and west Pacific warm saline pools [37-40]. Thus, our transect is in an evaporative region with fresh warm pools to both the east and west. It suggests NH and SH Ekman currents at 50-150m combine to decrease the eastbound EUC core current. This is a small equatorial convergence. Two weaker narrow subsurface eastbound counter currents (SSCC and NSCC) are found at depth >150m at ~±4º latitude. This hints at potential additional deeper cell structures.

Mean Ekman surface currents from observed daily mean resolved zonal and meridional 10m-windspeeds are shown in Figure 7. Equatorial divergence is clearly shown with a NH northbound mean flow of 1.6±1.0cms^{-1} and SH southbound flow 2.3±0.7cm s^{-1}. This is similar to Ekman divergence reported in the upper 25m at 2ºN 140ºW in 2004-5 [41].

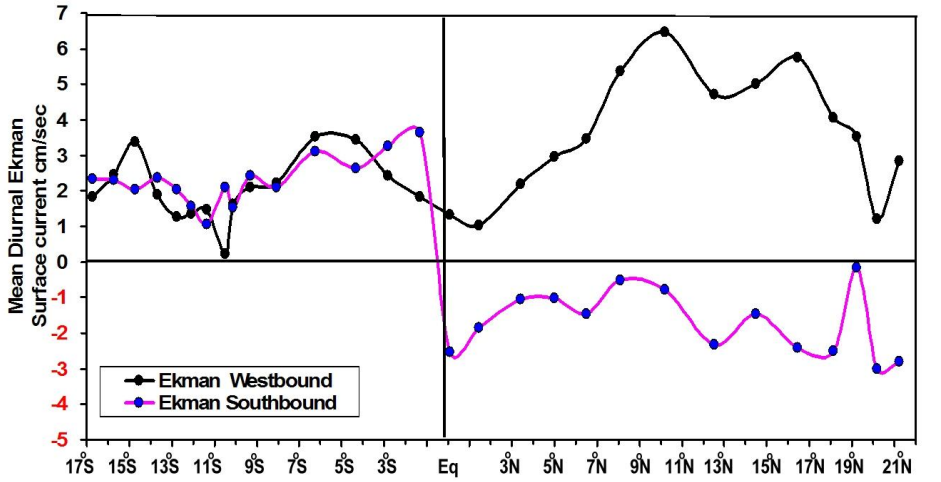

Figure 7 Computed Ekman zonal and meridional surface currents from daily mean 10m winds 17ºS-21ºN

Mean zonal surface currents are all westbound as expected in the Turtle and Heyerdahl westbound gyres. They are 2.1±0.9cm/s In the SH, and 4.0±1.5cm s^{-1} in NH. Peak current of ~6.5cm s^{-1} (~3nm day^{-1}) at ~11ºN is along the temperature front (Figure 3). It compares with the long-term SH and NH ocean gyre mean speeds ~6.2nm day^{-1} and ~5.9nm day^{-1} respectively (Figure 5). Thus, the ambient wind field generated about 50% of the long-term gyre speeds. This suggests winds were below average for the region during the research cruise. Our winds averaged 5.6±1.6m s^{-1} in SH and 8.1±2.4m s^{-1} in NH or 6.7±2.3m s^{-1} overall. This suggests mean winds ~10-15m s^{-1} produce the observed mean Ekman zonal currents.

We observed westbound winds of 7.1m s^{-1} the equator and show computed Ekman meridional and zonal depth profiles for this 10-m zonal windspeed (Figure 8). (We use the term ‘bound’ to distinguish wind directions usually quoted in terms of ‘from’ direction to current directions usually quoted in terms of ‘towards’ directions or ‘setting’).

ISSN 2347-3487

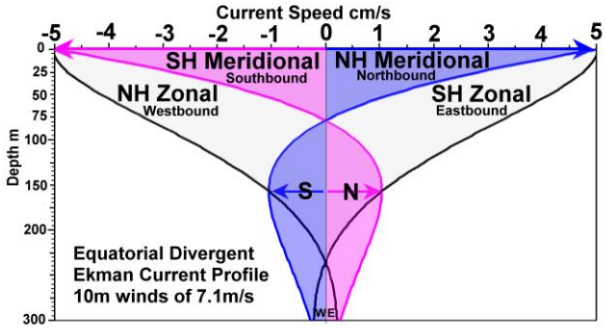

Figure 8 Computed zonal and meridional current profile for observed mean 7.1m s^{-1} west winds at equator

Note that surface drift at 3% of wind speed (shown in Figure 5 left) is higher than computed Ekman drift and at 3-4º to right (NH) rather than the 45º in Ekman transport. The two are equal from about 2m-depth. This suggests the 3m-depth is a suitable reference level away from the strong boundary layer drift current regime.

Ekman meridional divergence extends to ~75m. The speed is linearly scaleable with windspeed, but the divergence/convergence boundary depth remains stable. Maximum equatorial convergence below ~75m is only 20% of the peak surface current and is found at ~150m.

Zonal westbound Ekman currents extend to ~250m depth with only a very weak deeper eastbound component. This suggests the eastbound 140cm/s core of the EUC and the reduced speed ~80cms^{-1} central core is maintained by Ekman convergence at ~150m. Observed equatorial upwelling of 1.6m day^{-1} would require ~62d or ~2 months to bring water from 100m to surface [42]. This is the same age reported for surface waters from other brine producing regions. It suggests observed vertical transport derives from the balance between the brine settlement rate and wind-driven upwelled replacement water. Maximum upwelling of 2.3×10^{-5}m s^{-1} (~2m day^{-1}) at 60m above the same high speed EUC core was observed in a detailed current meter array experiment at 140ºW [43].

2.2 Meridional depth profiles of temperature, salinity and density

CTD profiles were mostly taken within about an hour of local noon. They are therefore representative of conditions near maximum surface evaporation. The temperature profile to 300m from 17ºS to 20ºN is shown in Figure 9 with temperatures of 28°C and 25°C highlighted. The 28ºC isotherm is at the surface from ~2.5ºS to ~9ºS where it deepens to ~75m forming a warm pool (Figure 9).

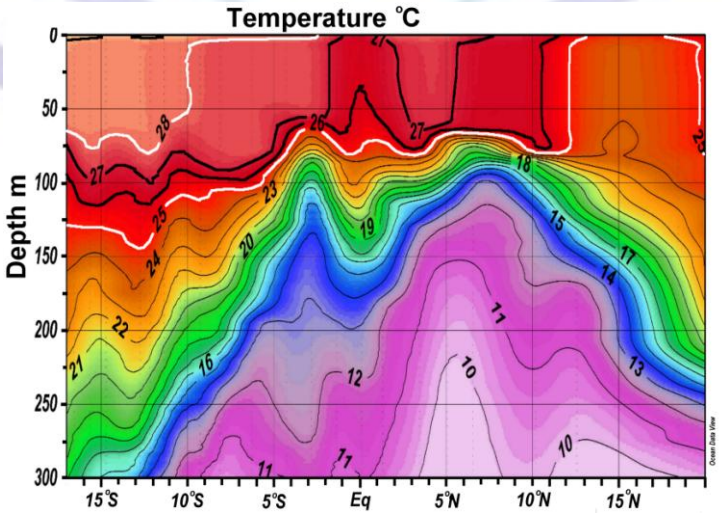

Figure 9 Meridional temperature profile to 300m 17°S-20°N with 28°C and 25°C highlighted

The 25ºC isotherm is at the surface ~20ºN to ~12ºN where it deepens to ~75m crossing the equator to fall to ~125m under the warm pool from ~12ºS. The cold tongue ~27ºC water is seen ~2ºS-2ºN down to ~50m where a warm water core coincides with the EUC. Cold ~15ºC isotherms form wave crests at ~100m depth at ~5ºS, 1ºN and 6ºN corresponding to suggested upwelling zones in the current profile. The strongest upwelling of alpha/beta frontal water of ~10ºC is at ~225m at 6ºN and ~275m at ~13ºN. This suggests feedback from the North Pacific upwells north of the equator.

Meridional salinity profile is shown in Figure 10 with salinity of 36.4‰ and 34.2‰ are highlighted. Isohalines are near vertical in the upper 75m corresponding to Ekman meridional mixing and a beta salt stratified regime.

The 3m-salinity gradient south-to-north is high-to-low (>36.4 to <34.4‰). The 34.8‰ isohaline is near vertical to ~300m just north of the equator marking a division between two haline regimes. SH mean maximum salinity is remarkably constant at ~36.4‰ at ~100m. By contrast the NH maximum salinity varies from the surface to ~170m with a minimum water column salinity ~34.3‰ at ~85m at ~6ºN suggesting upwelling cold brackish water.

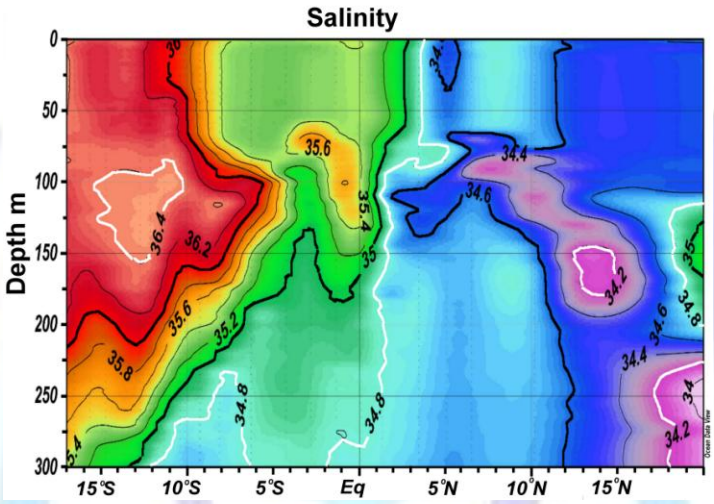

Figure 10 Meridional salinity profile to 300m 17°S-20°N with 36.4‰ and 34.2‰ highlighted

The SH and NH have independent density regimes (Figure 11). The 22.3 isopycnal (highlighted) is at the surface south of

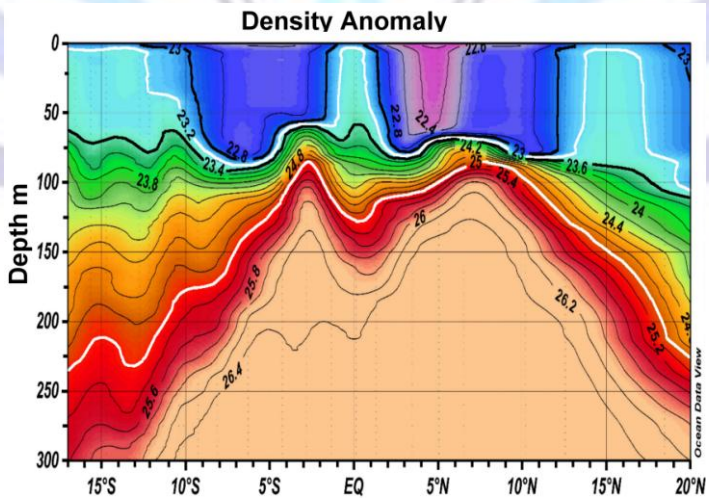

Figure 11 Meridional density profile to 300m 17°S-20°N with 23.2 and 25 highlighted

12ºS,the 22.3 isopycnal (highlighted) is at the surface south of 12ºS, within ±1º of equator and at ~11-14ºN at the frontal zone. This suggests isopycnal balance north and south of the equator with no net meridional exchange. The potential density from these temperature-salinity profiles shows distinct troughs marked by the 22.3 isopycnal in both the SH and

NH. Below about 100m the density gradient is poleward. The 25.0 isopycnal (highlighted) at ~100m depth at 3ºS descends southwards to ~220m at 15ºS in warm salty water. It forms an equatorial trough 3ºS-8ºN down to ~125m at the equator corresponding to the EUC. From 8ºN it descends northwards to ~225m at 20ºN in cold brackish water. This suggests a SH southward warm brine flux below ~100m and a similar flow northward in NH. Thus, equatorial brine flows poleward in both hemispheres to complete the global circulation scheme [17]. Two distinct water masses lie either side of the front at ~11ºN.

2.3 Southern hemisphere 17-2ºS diurnal temperature and heat cycles

Mean meridional SH hourly temperatures over 14 complete 24hr days correspond to the solar radiation cycle (Figure 12).

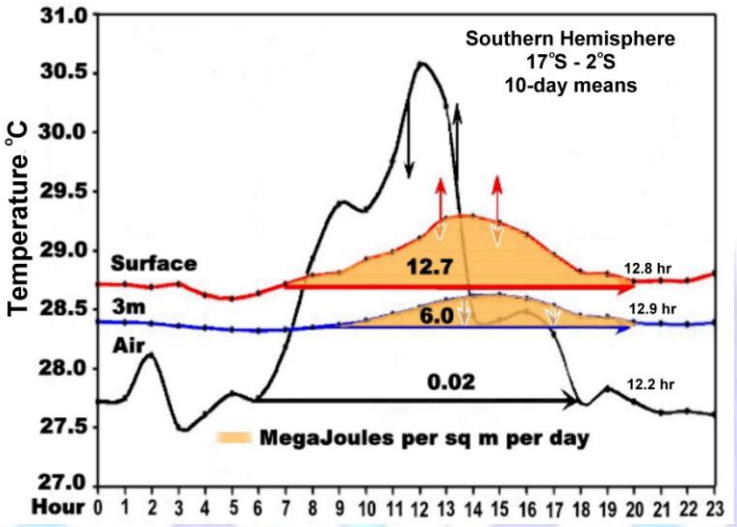

Figure 12 Southern Hemisphere 10day mean heat cycles

In the morning heating phase, solar radiation warms the surface and 3m layers. Air is colder than surface or 3m temperatures outside the normal tropical 06:00-18:00 LT diurnal solar heating cycles. By 09:00 LT air is warmer than the surface layer. Sensible heat exchange is suggested by air-cooling between 09:00-10:00 LT. This has negligible impact on the SST because of the ~3,000x greater seawater heat capacity. From ~10:00 LT heating continues in all layers.

In the afternoon cooling phase, the surface layer loses heat by upward radiation and evaporation and downward through brine-induced thermohaline sinking. There is a similar sensible heat exchange between about 14:00-16:00 LT when the seawater is warmer than air. The 3m layers have downward-only heat transport - thermal diffusion during the heating phase and thermohaline sinking during later cooling. This forms a heat trap and a direct measure of ocean heating. There is no evaporation from 3m and no precipitation content unlike at the air-sea interface.

Maximum temperatures were reached in dry air around noon, in surface at 13.4±0.5 LT and at 3m 14.6±1.3 LT. Buckets sample the upper ~0.2m. Gradients can exist over the upper 1m but we take them to be representative of the upper ~1m bulk temperature [8-9]. This suggests thermal diffusion of heat from the ~0.2m surface layer to 3m occurs in the morning since surface density is still decreasing. We calculate over ~2.8m the thermal eddy diffusion over ~1.2±0.5hrs to be ~6.5±1.8x$10^{-4}$$m^2s^{-1}$. Thermal diffusion is usually difficult to distinguish from thermohaline vertical flow that is important in double diffusion processes [44]. It is in the range of thermal eddy diffusivity ~1-10x$10^{-4}$$m^2s^{-1}$ reported in the California Current [45].

Diurnal heat fluxes (the area above the base temperature of the curves in Figure 12) were calculated to be: 1) through the surface ~18.2±0.8M $m^{-2}day^{-1}$, and 2) through the 3m layer ~6.1±0.4MJ$m^{-2}day^{-1}$. This suggests that sequestration of ~33% of surface heat through 3m layers into the deeper ocean. Air has a comparatively trivial heat cycle of 19.2±1.1kJ$m^{-2}day^{-1}$.

ISSN 2347-3487

2.4 Southern hemisphere evaporation salt and density cycles

The mean daily SH salinity cycle along the meridional cruise track is shown in Figure. 13.

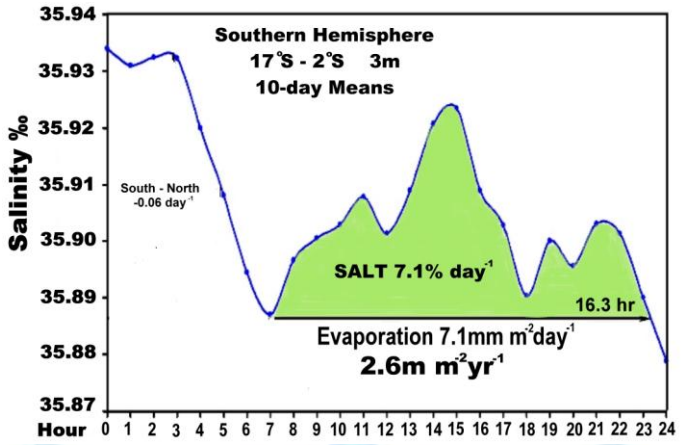

Figure 13 Southern Hemisphere 10day mean salt cycles

The S-N salinity reduction and the 9.9h daily solar radiation evaporation cycle are clearly visible. We calculate mean daily evaporation from the diurnal salinity enhancement (again the area under the 9.9h curve) to be 7.3mm m^2day^{-1} or ~2.67myr^{-1}. This the same order as the SH evaporation reported at ~34ºS in the Australian Murray River basin [46]. We calculate that ~17.85MJm^{-3} is needed to evaporate ~7.3mm $m^{-2}day^{-1}$. This suggests a potential further surface warming of ~4.5ºCm^{-3} were it not lost to evaporation i.e. a potential SST ~33ºC. SH evaporation and surface heating total ~36 $MJm^{-2}day^{-1}$. Thus, the ~6.1$MJm^{-2}day^{-1}$ passing below 3m is ~17% of the total surface heat while evaporation takes ~50% and the remainder is lost to the atmosphere. Evaporative heat loss and trapped heat total ~24$MJm^{-2}day^{-1}$ or ~67% of the total surface heat.

The daily density flux over the 14.3hr cycle is ~0.5$kgm^{-3}day^{-1}$ for a vertical flux ~$10^{-5}ms^{-1}$ (Figure 14).

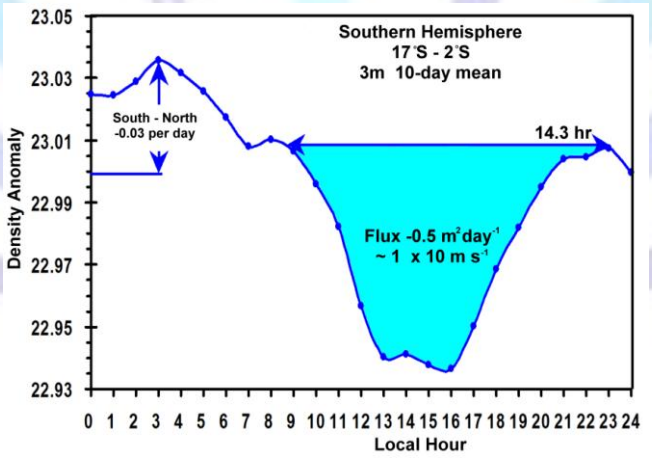

Figure 14 Southern Hemisphere 10day mean density cycles

The density flux runs over a longer cycle than the salt flux because it is in two parts. First there is density increase through evaporation then it continues from cooling after sunset. The S-N trend is –0.03kg $m^{-2}day^{-1}$ because the profile excludes equatorial higher density upwelled water with a balancing increasing gradient.

We calculate mean vertical mass diffusion as ~1±0.8x$10^{-5}ms^{-1}$ over the 14.3hr cycle or 0.5$mday^{-1}$. The mean maximum rate was –0.07$kgm^{-3}hr^{-1}$ or -2x$10^{-5}ms^{-1}$ or -1.0$mday^{-1}$. This compares with Perez et al. [47] downwelling –0.8$mday^{-1}$ at ~5ºS and –1.4 $mday^{-1}$ at ~7ºN with equatorial upwelling ~1.6$mday^{-1}$. This suggests warm salty water at the bottom of 75m

cells would take ~60-100 days (~2-3 months) to descend. This is similar to the age of water reported for the Great Barrier Reef [48]. Over the same time period upwelled water would come from depths ~100-150m that would be drawn from water <19ºC on our transect. The upwelling regions are clearly suggested by waves on the thermocline contours (Figure 9)

2.5 Northern hemisphere 3.4-21.2ºN diurnal temperature and heat cycles

We separated the NH into two regions either side of the strong front, from 3.4-8.1ºN and from 12.5-21.2ºN. The 3m heat capture was similar for both regions at ~12.3 and 11.3MJ m^{-2} day^{-1}, but ~9% lower than in the SH (Figure 15 a, b).

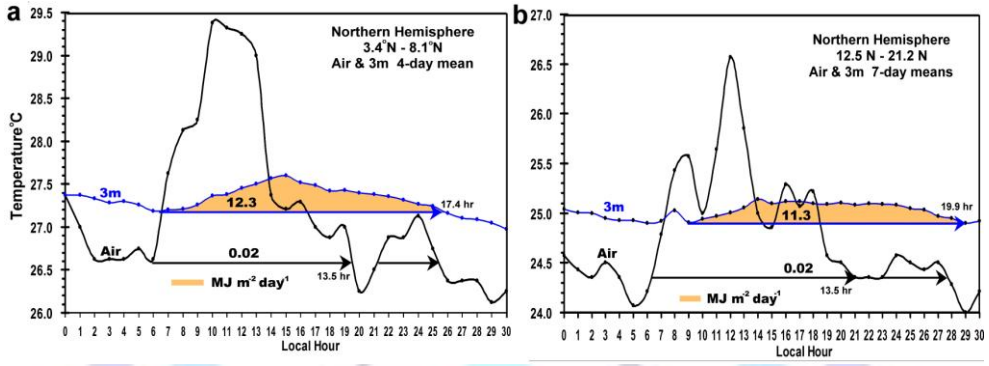

Figure 15 Northern hemisphere temperature and heat cycles a) 3.4-8.1ºN and 12.5-21.2ºN

It is double the heat capture found in the SH. This suggests stronger thermohaline convection. The mean temperature difference between the two regions is ~2.4ºC with 2.5hr longer diurnal cycle. Based on thermodynamics of the Clausius-Clapeyron relationship this suggests ~17% lower evaporation at the rate of 7%ºC^{-1}[1]. We observed only about half that reduction. Clearly another process is important in heat capture in addition to surface evaporation.

The air heat cycle is ~8% lower at ~18.3 and 22.9kJm^{-2}day^{-1}. The distinct cycle in the morning for the more northerly air temperature suggests significant sensible heat loss to the surface ocean during the warming phase. This is more pronounced after sunset when the 3m water temperature is ~1.5ºC higher than air temperature. The warming night arrows in Figure 15 mark air and diurnal solar cycle. Lower evaporation and surface warming is a consequence of the lower surface temperatures and thus vapor pressure (Clausius-Clapeyron relation). However, its effects are also limited by seawater density that governs sinking rates and radiative balance. Nighttime radiation heat loss from the ocean surface depends on cloud cover. Only in the northern hemisphere 12.5-21.2ºN did we find correlation with nighttime clear sky in oktas discussed below.

2.6 Northern hemisphere evaporation and salt cycles

Total evaporation for both NH regions averages ~4.5mm m^{-2}day^{-1} or ~1.64myr^{-1}, i.e. ~1m less than in the SH (Figure 16).

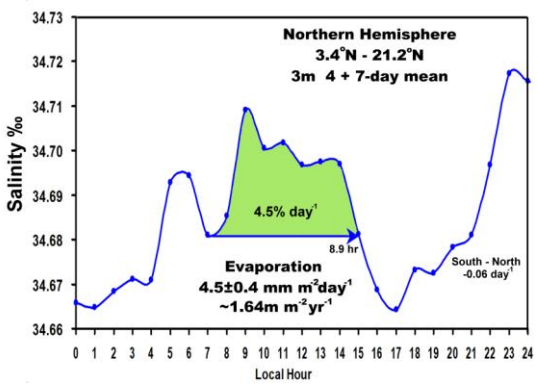

Figure 16 Northern hemisphere salt cycles 3.4 - 21.2ºN

Both NH regions either side of the frontal zone show diurnal salt cycles with rising salinity toward midnight and northwards. We calculate ~11.0MJ m^{-2} day^{-1} is needed to evaporate ~4.5mm m^{-2} day^{-1}. We do not know the surface flux without bucket samples. However, the mean NH evaporative heat and 3m flux total ~22.6MJ m^{-2} day^{-1}. This compares well with SH evaporative heat loss and trapped heat total of ~24MJ m^{-2} day^{-1}. This is 6% lower and on thermodynamic principles could occur from ~1ºC colder surface temperature. Therefore, it is not determined from purely thermodynamic drivers.

We arrive at a surprising finding that heat trapped below 3m plus evaporative heat are roughly the same in the NH and SH but the ratios 2:1 are reversed. The SH has higher evaporation, 2.6: 1.6myr^{-1}. The NH has higher heat sequestration 11.8: 6.1$MJm^{-2}day^{-1}$. NH evaporation is higher than the 1.4myr^{-1} measured a decade earlier in the eastern warm pool [49]. However, our central Pacific location is a source region for evaporation that is carried on Walker zonal cells to precipitation in eastern and western warm pools. The steady evaporation of the topics results in concentrated precipitation in the warm pools of 4.5myr^{-1} [49]. Moreover, our observed evaporation rate is consistent with the ~1.6myr^{-1} reported for 2002-4 at ~28ºN in a Florida coastal lagoon [50].

2.7 Evaporation correlation of wind speed, humidity and clear sky radiation

We looked for single variable correlations between observed evaporation and bulk parameters. Evaporation is usually assumed dependent on windspeed and relative humidity calculated from standard meteorological parameters [51-52]. There are few, if any, experimental scientific timeseries verification data [12]. A persistent evaporation-produced conductive moist air layer 5-10m is successfully used as a radio communications channel above the Great Barrier Reef tropical shelf sea [53]. It was found by trial and error but attests to year-round evaporation in a hypersaline tropical sea [48]. However, there has been no hourly timeseries verification similar to our mid-Pacific experiment. Since these bulk parameterizations are widely used we ran correlation analyses looking for single variable dependencies.

We found low correlation (~0.3-0.4) between SST for mean wind speeds averaging ~20kt (~10m/s), <10m/s in the SH, and mean relative humidity ~90% in both NH and SH. Several authors report that diurnal turbulent mixing regime was suppressed at wind speeds below <5m/s [12, 54]. None recognize that evaporation is an exponential function of temperature related by the Clausius-Clapeyron relation to saturation vapor pressure [1]. Moreover, seawater density including both temperature and salinity has been neglected in previous formulations.

We expected cloud cover to show significant correlations to solar radiation through the diurnal cycle. However, similar low correlations to SST were found for mean clear sky percentages calculated from observed oktas that averaged ~60% for both day and night. Negligible correlations were found during the diurnal evaporative cycle computed separately from nighttime cloud cover. The one exception was for the NH region south of Hawaii where mean clear sky ~37% had –0.8 correlation to evaporation as measured as a function of salt sequestration. Thus, cloud cover significantly reduced daytime radiative input or nighttime heat loss. This probably accounts for the similarity of observed salt sequestration in the two NH regions despite their temperature difference ~2°C. The NH is in the temperature-dominant low salinity region of the alpha/beta salt/heat circulations though heat and salt cycles were irregular; evaporation was substantially the same throughout.

This confirms the importance of considering cloud cover along with sea surface temperature and salinity in evaporation and heat sequestration [1]. Relative humidity and windspeed are not relevant. Water vapor is a gas that expands from liquid into gas. Relative humidity is only rarely of significance. This suggests that the observed mean 90% relative humidity in the SH and NH leaves room for more water vapor in a warming atmosphere. Water vapor is lighter than air and naturally rises on evaporation. We observed several instances of transfer of heat to air from sea. This was visible in air temperatures but not in water temperature because of the 3000x greater heat capacity. Nocturnal radiative heat loss is important in the lower salinity NH where heat can be sequestered into the ocean until just before dawn. This is an important seasonal mechanism in the northern Gulf of California where winter cooling can produce brine pulses [55]. Gulf circulation is tidally pumped by strong tides. This contributes to year-round outflow to the ocean at about 500m and is

important for the seasonal heat balance [56]. It contributes brine to North Pacific under the Turtle gyre in contrast to Mediterranean brine outflow to the Atlantic Ocean that is seasonal and at ~1500m.

The markedly different SH and NH hemisphere heat sequestration is a consequence of estuarine density stratification not evaporation. Moreover, evaporation does not depend on windspeed and relative humidity in the widely used coefficients from standard meteorological observations [51, 52]. Measurements are based on pan evaporation over land. The daily solar heating cycle is the clear driving mechanism by changing water vapor pressure every second over the solar cycle. Daily averages of bulk parameters are too coarse compared to actual hourly or better timeseries.

2.8 Tropical zonal heating

We assume tropical heating is constant year-round to estimate the annual trapped heat flux to be ~4.7x10^{22}Jyr^{-1} over SH tropics. This is based on mean flux of 6.1MJm^{-2}day^{-1} over the ~1,650km meridional track 17.1ºS-2.0ºS and a Pacific Ocean zonal width is ~7,000nm or 1.3x10^{7}m for daily total meridional heat flux is ~1.3x10^{20}J day^{-1}. Similar calculation for the NH heating yields a trapped heat flux of ~11.8x10^{22}Jyr^{-1}. This is based on ~11.8 MJm^{-2}day^{-1} over ~2,100 meridional km, 3.4-21.6ºN, for a downward heat flux of ~25x10^{12}m^{-2}day^{-1} or daily total meridional heat flux ~3.3x10^{20}J/day. Thus, the combined SH and NH data suggest a trapped heat flux ~1.6x10^{23}Jyr^{-1} between Tahiti and Hawaii. This is likely to be biased high because evaporation from fresh warm pools will not result in subsurface heat sequestration.

Levitus et al. [2] estimate of world ocean heat content for 0-700m layers that increased from 1955-2010 by 16.7±1.6x10^{22}J at a rate of 0.27Wm^{-2} and a trend of +4.0x10^{21} Jyr^{-1}. Their earlier estimate of ocean heat was an increase of ~2x10^{23}J from 1955-1995 for a mean ocean warming of 0.06ºC [54]. Clearly, these estimates are based on sparse data before the mid-1990s, are global estimates with little data from mid-Pacific and are averaged over upper 100m. However, they are broadly supportive of the Challenger data that showed +0.6ºC in surface temperatures and +0.4ºC below [6].

2.9 New meridional tropical counter-rotating cell regime

We calculated the meridional geostrophic regime from midnight to midnight to be mostly free of diurnal variation (Figure 17). The hourly data allows resolution of currents that are at least an order of magnitude smaller then zonal currents. Alternate divergent upwelling/convergent downwelling sites mark meridional cells (Figure 17 and Table 1).

We found cells throughout the region from Tahiti to Hawaii in addition to the pair either side of the equator reported by Perez et al. [47]. The strongest divergence was the equatorial water with strong flows to the north and south. Upwelled water (26.4ºC, 35.4‰, 23.25) flows northbound at a peak 0.32cms^{-1} (~3kmday^{-1}) in the ~590km long Northern Tropical Cell (NTC) and at 0.18cm cms^{-1} (~1.5kmday^{-1}) southbound in ~626km Southern Tropical Cell (STC). It suggests surface residence times ~200-400days.

However, we find these meridional tropical cells (MTCs) are each half of a pair of counter-rotating cells between two divergent upwelling zones. For example, the ~600km-long Southern Counter Cell 1 (SCC1) upwells water (28.5ºC, 36.2‰, 23.24) at ~11ºS that also flows northbound to the STC downwelling site at peak current 0.38cms^{-1} (~3kmday^{-1}). It forms a balanced pair over ~1230km, forming a geostrophic valley in the South Pacific Subtropical Heyerdahl gyre (see Figure 5 for all named gyres).

Moreover since the upwelled water at 11.1ºS also travels southbound to another downwelling site, there is no net meridional flow across cell pairs. There are fronts between water masses at the same density but with different balancing temperature and salinity [1]. This applies to all cell pairs. It is particularly strong for NTC and STC equatorial upwelled cells that form separate SH and NH warm and cold cell pairs. Coriolis divergence of upwelled cold water forms a permanent barrier along the equator. Other upwelling sites are weaker and probably vary with shifts in wind regime. However, they are similar to the surface drift barrier reported in the north Atlantic from the Gulf Stream that prevents further southwards penetration of Arctic brackish water beyond about 50ºN and is thus clearly a feature of meridional overturning cells [26].

ISSN 2347-3487

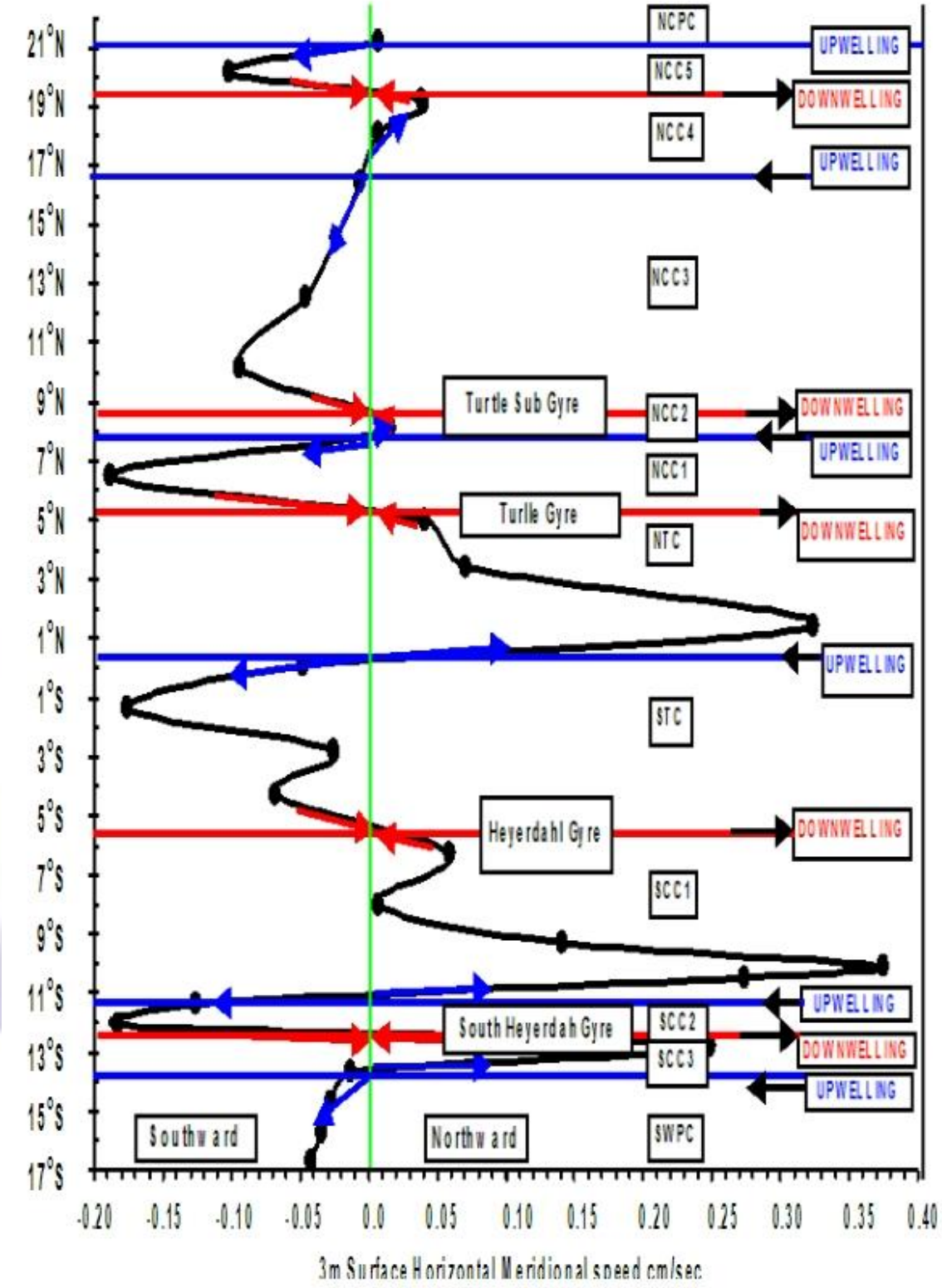

Figure 17 Tropical meridional currents, vertical cells, upwelling (blue), downwelling (red) sites and gyres

The NH has three counter-rotating cell pairs of ~890km, 1030km and 430km with flows mostly southwards to downwelling sites at 9ºN and 5ºS. Here the Coriolis effect is unidirectional so upwelled water follows density gradients most strongly southbound. The northernmost upwelling water, (24.8ºC, 35.1‰, 23.5), at 21.2ºN has slightly higher density than

ISSN 2347-3487

equatorial upwelled water. The very weak downwelling at 9ºN and upwelling at 8ºN are associated with the front at 11ºN and show net southward flow.

Table 1. Tropical cell upwelling and downwelling properties and Equatorial Under Current (EUC) core details. Cells names are Southern Warm Pool Cell (SWPC), Southern Counter-rotating Cell (SCC), Southern and Northern Tropical Cells (STC, NTC), Northern Counter-rotating Cell (NCC), and Northern Cool Pool Cell (NCPC).

Cell		Date	Hr	Lat.	Long.	T ºC	S ‰	σ kgm^{-3}	Cell km	Cell Pair
NCPC	End	13 June 2008	0	21.6	-157.3	25.53	35.02	23.18	44	
NCC5	Up	12 June 2008	9	21.2	-156.8	24.80	35.11	23.49	201	433
NCC4	Down	10 June 2008	14	19.4	-154.5	25.07	34.54	22.91	232	
NCC3	Up	8 June 2008	22	17.3	-152.6	24.85	34.55	22.99	964	1033
NCC2	Down	4 June 2008	19	8.6	-147.4	27.23	34.78	22.42	69	
NCC1	Up	4 June 2008	10	8.0	-146.9	27.04	34.75	22.46	304	893
NTC	Down	2 June 2008	17	5.3	-144.5	27.86	34.47	21.94	589	
Equator	Up	30 May 2008	8	-0.0	-142.1	26.38	35.42	23.25		
STC	Down	26 May 2008	19	-5.6	-141.2	27.90	35.19	22.55	626	1228
SCC1	Up	17 May 2008	21	-11.1	-144.9	28.47	36.21	23.24	602	
SCC2	Down	15 May 2008	23	-12.4	-147.0	28.56	36.12	23.13	149	290
SCC3	Up	14 May 2008	14	-13.7	-148.2	28.84	36.35	23.23	141	
SWPC	Start	10 May 2008	23	-17.1	-149.8	28.61	36.14	23.13	384	
		Northern Front							**Front km**	
Front	North	6 June 2008	17	13.0	-150.0	24.96	34.45	22.87	482	
Front	South	4 June 2008	19	8.6	-147.4	27.23	34.78	22.42		
Front Max	South	5 June 2008	22	11.1	-149.0	26.41	34.83	22.74	12.2	
Front Max	North	5 June 2008	21	11.2	-149.1	25.31	34.52	22.82		
EUC		**Equatorial Under Current**							**Depth m**	**cm/s**
Core		30 May 2008	8	-0.0	-142.1	20.75	35.50	25.00	125	140

Separate meridional circulation suggests that the equatorial divergent upwelling and the EUC cause NH and SH to have separate circulation systems. This equatorial asymmetry supports the suggestion of a trans-equatorial circulation bottleneck in climate models [57]. We noted earlier that the EUC has an elongated annular cylindrical section with 140cm/s eastbound flow. The counter-rotating cells STC and NTC feed into the EUC to produce an Ekman westbound flow below 75m. This reduces the core EUC eastbound current to ~80cm/s. This appears to be the only location where NH and SH surface waters mix. Moreover, it travels eastward in EUC and plays no part in surface gyre transportation. Thus, it supports the concept of north Pacific as a global-scale estuary with the only outlet through the Bering Strait. The south Pacific exhibits a separate hypersaline estuarine circulation with higher evaporation with warmer and more saline surface waters.

The NH has three counter-rotating cell pairs of ~890km, 1030km and 430km with flows mostly southwards to downwelling sites at 9ºN and 5ºS. Here the Coriolis effect is unidirectional so upwelled water follows density gradients most strongly southbound. The northernmost upwelling water, (24.8ºC, 35.1‰, 23.5), at 21.2ºN has slightly higher density than

equatorial upwelled water. The very weak downwelling at 9ºN and upwelling at 8ºN are associated with the front at 11ºN and show net southward flow.

Table 1. Tropical cell upwelling and downwelling properties and Equatorial Under Current (EUC) core details. Cells names are Southern Warm Pool Cell (SWPC), Southern Counter-rotating Cell (SCC), Southern and Northern Tropical Cells (STC, NTC), Northern Counter-rotating Cell (NCC), and Northern Cool Pool Cell (NCPC).

Cell		Date	Hr	Lat.	Long.	T ºC	S ‰	σ kgm^{-3}	Cell km	Cell Pair
NCPC	End	13 June 2008	0	21.6	-157.3	25.53	35.02	23.18	44	
NCC5	Up	12 June 2008	9	21.2	-156.8	24.80	35.11	23.49	201	433
NCC4	Down	10 June 2008	14	19.4	-154.5	25.07	34.54	22.91	232	
NCC3	Up	8 June 2008	22	17.3	-152.6	24.85	34.55	22.99	964	1033
NCC2	Down	4 June 2008	19	8.6	-147.4	27.23	34.78	22.42	69	
NCC1	Up	4 June 2008	10	8.0	-146.9	27.04	34.75	22.46	304	893
NTC	Down	2 June 2008	17	5.3	-144.5	27.86	34.47	21.94	589	
Equator	Up	30 May 2008	8	-0.0	-142.1	26.38	35.42	23.25		
STC	Down	26 May 2008	19	-5.6	-141.2	27.90	35.19	22.55	626	1228
SCC1	Up	17 May 2008	21	-11.1	-144.9	28.47	36.21	23.24	602	
SCC2	Down	15 May 2008	23	-12.4	-147.0	28.56	36.12	23.13	149	290
SCC3	Up	14 May 2008	14	-13.7	-148.2	28.84	36.35	23.23	141	
SWPC	Start	10 May 2008	23	-17.1	-149.8	28.61	36.14	23.13	384	
		Northern Front							**Front km**	
Front	North	6 June 2008	17	13.0	-150.0	24.96	34.45	22.87	482	
Front	South	4 June 2008	19	8.6	-147.4	27.23	34.78	22.42		
Front Max	South	5 June 2008	22	11.1	-149.0	26.41	34.83	22.74	12.2	
Front Max	North	5 June 2008	21	11.2	-149.1	25.31	34.52	22.82		
EUC		**Equatorial Under Current**							**Depth m**	**cm/s**
Core		30 May 2008	8	-0.0	-142.1	20.75	35.50	25.00	125	140

Separate meridional circulation suggests that the equatorial divergent upwelling and the EUC cause NH and SH to have separate circulation systems. This equatorial asymmetry supports the suggestion of a trans-equatorial circulation bottleneck in climate models [57]. We noted earlier that the EUC has an elongated annular cylindrical section with 140cm/s eastbound flow. The counter-rotating cells STC and NTC feed into the EUC to produce an Ekman westbound flow below 75m. This reduces the core EUC eastbound current to ~80cm/s. This appears to be the only location where NH and SH surface waters mix. Moreover, it travels eastward in EUC and plays no part in surface gyre transportation. Thus, it supports the concept of north Pacific as a global-scale estuary with the only outlet through the Bering Strait. The south Pacific exhibits a separate hypersaline estuarine circulation with higher evaporation with warmer and more saline surface waters.

ISSN 2347-3487

2.10 Evaporation, critical or limiting temperature, salinity and density

In order to examine details of the critical buoyant surface water of density 22.0 at 5.3°N and 22.6 at 5.6°S is found in the gyre downwelling regions (red). Upwelling regions (blue) have higher density in the range 22.6-23.3.

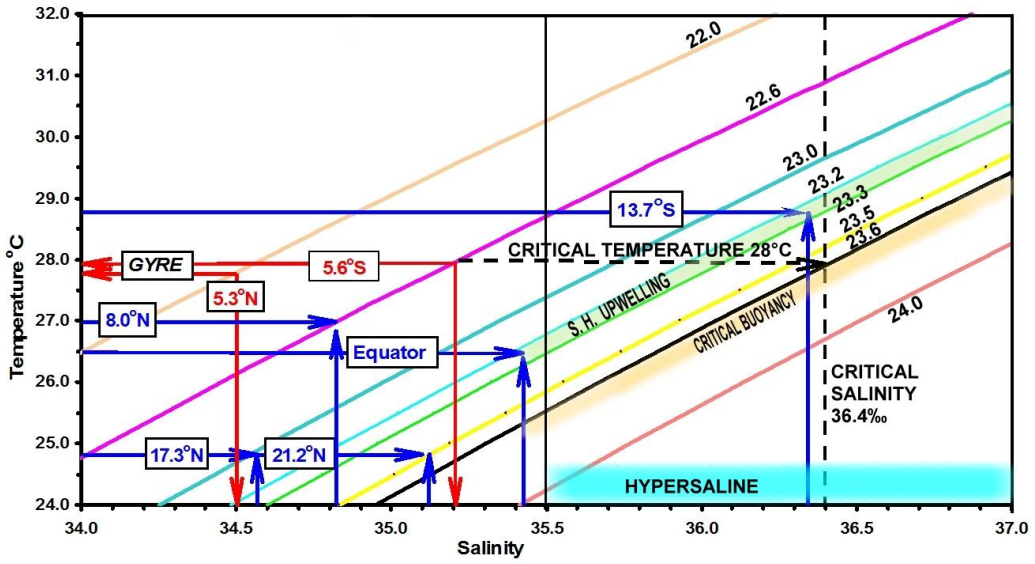

Figure 18 Central equatorial Pacific TS diagram of upwelling, downwelling, and gyres.

We found the critical transition to salt dominated sinking was salinity <36.4‰ and temperature of <28°C Seawater density increases with increasing salinity but decreasing temperature. At salinity 35‰ the second order term in the density equation changes sign [1, 33]. This is increases the significance of salinity to that of temperature. This confirms that densities as well as evaporation are important factors in evaporation and ocean heat sequestration.

3 DISCUSSION

Thermodynamic processes are summarized in on the 200m-temperature depth profile with top 5m on exaggerated pycnoclines (Figure 19) [1]. Upwelling (blue) follows thermocline upward trending contours. Downwelling (red) connect at

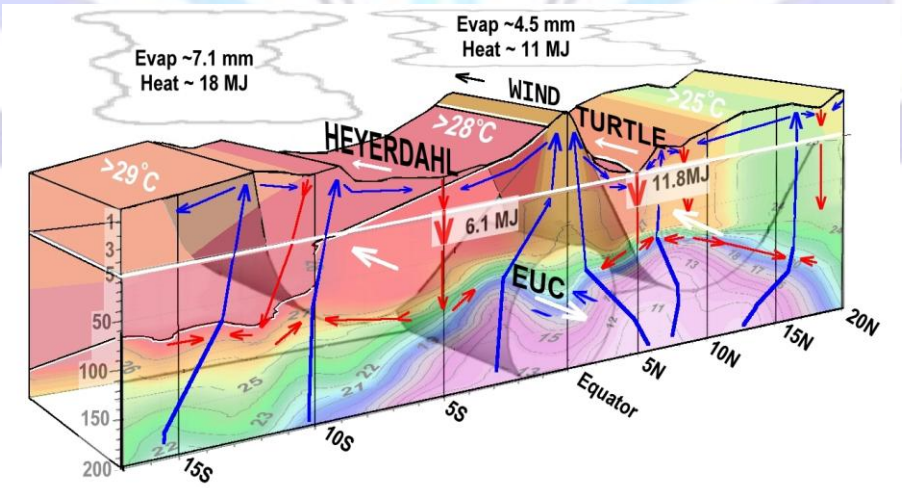

Figure 19 Tropical circulation schematic of surface layer processes and daily fluxes.

Ekman meridional current reversal depth ~75m (Figure 8). The exaggerated surface layer pycnoclines emphasise meridional flows from upwelling geostrophic mountains in gyre downwelling valleys that determining cell circulation. Cold

water warms, evaporates and becomes denser on the surface over 200-400 days. Downwelling sites of sinking brine have characteristics of rip currents that carry accumulated fluxes away from convergence zones (Figure 17).

The most striking result is the north-south asymmetry across the equator. Evaporation and consequent precipitation is higher in the southern hemisphere. However, heat trapped in below 3m is much twice as much in the north as in the south Pacific. We believe significant finding has great significance for anthropogenic global warming [1].

3.1 Top of ocean boundary layer evaporation and brine production

Sea surface boundary layer physical processes and properties account for all observed anthropogenic global warming. Figure 20 shows the surface freshwater down to hypersaline brine from Polar Regions to the tropics. Two controlling equations for evaporation and density as a function of temperature are shown with our timeseries findings [1].

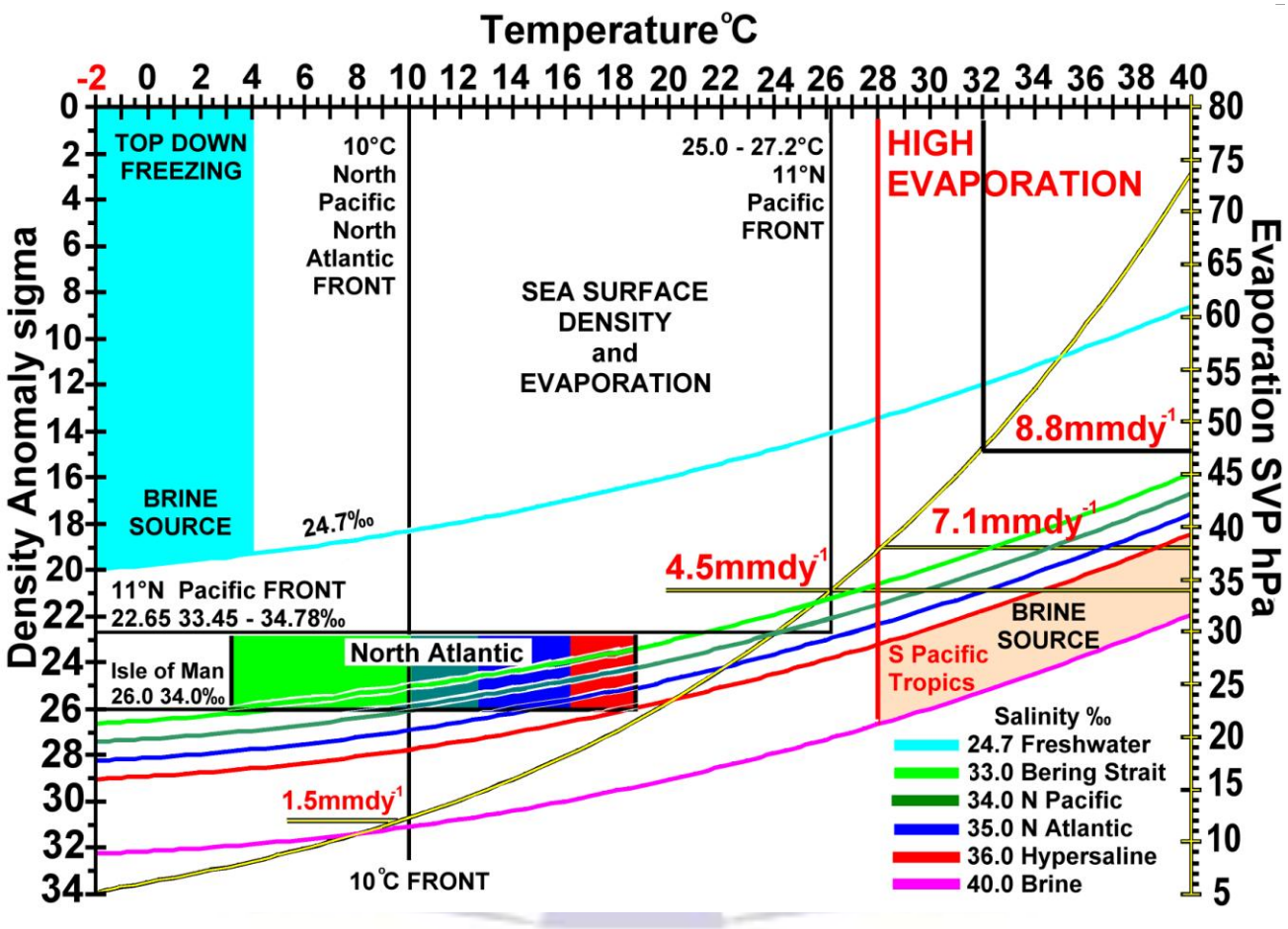

Figure 20 Clausius-Clapeyron evaporation and seawater density T-S diagram

Gill [33] gives surface seawater density, ρ kgm^{-3}, usually expressed as density anomaly from freshwater, σ (1-ρ), in the range 30≤S‰≤40 and -2≤T°C≤30 as

$\sigma = -0.17 + 0.808S - 0.756144T^2 - 0.002964T^2(35-S)$.

It is given in parts per thousand (‰) rather than practical salinity units (psu) used for deep water. The last term in the equation gives alpha/beta transition at 35‰<S>35‰. Evaporation derives only from the sea surface skin temperature (T°C) that controls the equilibrium or saturation vapor pressure, e_s, (hPa) expressed as the Clausius-Clapeyron relation,

$$e_s = 6.1094 \exp\left(\frac{17.625T}{T + 243.04}\right).$$

We use the physics definition of freshwater as water that reaches temperature of maximum density before freezing point with salinity 0-24.7‰ [1]. Freshwater or brackish water is also used to describe water with salinity 1 to <35‰ [17]. Drinking water has salinity <1‰. Standard seawater is defined as 35‰. Hypersaline was defined as salinity >35.5‰ [48]. The high evaporation zone >28°C and >36‰ is marked in red (Figure 20). This is a major brine formation region. Asymmetric heat trap results from the latent heat of evaporation seven times the heat of fusion (2442: 342 MJm^{-3}). Heat trapped by evaporation in the tropics is trapped by surface ice with $1/7^{th}$ the heat loss per unit volume.

The 11°N frontal system mean density and temperature are marked along with the measured ~4.5$mmday^{-1}$. It is has mean temperature 26.1°C and density 22.65 boundary between two water masses (Table 1). The fronts at 10°C in both the North Pacific have a pro-rated trivial 300% lower evaporation rate of ~4.5$mmday^{-1}$. The North Pacific front is limited by the low underlying salinity <35‰. The Isle of Man water masses are from Arctic meltwater and runoff as well as from the Gulf Stream tropical water [1]. The long-term average salinity is 34‰. But at density ~26 the salinity range is from brackish to hypersaline. There are consistent seasonal variations with pulses of high salinity and low salinity water [1]. Indeed, salinity higher than <36‰ were recorded in the daily surface timeseries between 1992-1996. Pulses of cold surface waters were associated with strong westerly or northwesterly winds carrying water on the Viking gyre from the Newfoundland coast. Pulses of Gulf Stream water are associated with sustained southwesterly winds [1]. North Atlantic water was described as a barrier wall between these two water watermasses across the Viking and Columbus gyres (Figure 5) [26]. It is much stronger than the north Pacific front because of the wide range of surface water from polar and equatorial waters.

3.1.1 Tropical Evaporation

High evaporation at temperatures >28°C with evaporation 7.1$mmday^{-1}$ (2.6myr^{-1}) has saturated vapor pressure (SVP) 38hPa. Water ~32ºC has been observed for long periods in the western warm pool [58]. However, similar high temperatures were not found in the east Pacific warm pool before 2004 [59]. We pro-rated evaporation at 32°C and 47hPa to derive evaporation of 8.8$mmday^{-1}$ (3.2myr^{-1}). This suggests strong surface warming in regions confined by a subsurface halocline, leads to the reported ~7%$ºC^{-1}$ evaporation increase. This is likely to include the South Pacific tropics, but also the tropical north and south Atlantic, the land-locked north Indian Ocean as well as the Great Barrier Reef tropical shelf sea. Indeed recent analysis suggests a doubling of surface water warming trends in the 6yr records 2005-2010 compared to the 43yr mean 1960-2002 [60]. Argo floats have only recently been extended to sample in the upper 10m and confirm the warming trend [61].

The Araruama Lagoon (22ºS), with long-term mean salinity ~52‰ and surface temperature 28.4ºC, is a good indicator of trends. Unusually heavy precipitation in 1989-90 caused salinity to fall as low as 36‰ in this shallow south Atlantic lagoon [62]. It subsequently recovered but is ~2‰ salinity lower than its long-term value. Surface precipitation effectively puts a lid on the estuarine circulation to Ekman depth ~100m ensuring heat remains trapped. Enhanced precipitation has been ongoing for the last 25 years ago. High evaporation results only from temperature and therefore continues in Araruama Lagoon despite the reduction in salinity.

3.1.2 Southern hemisphere Evaporation and ENSO

Our data show the South Pacific Ocean is warming more slowly than the North Pacific but has high evaporation and higher potential precipitation. It suggests a slow weakening of the El Niño/Southern Oscillation (ENSO). ENSO is characterized by barometric pressure difference between Darwin (12ºS, 130.9ºE) and Tahiti (17.5ºS, 149.6ºW) that drives the Humboldt and SEC and the Heyerdahl gyre (Figure 5) [63-4]. On average the surface Humboldt Current warms from 15ºC at 40ºS to the ~28ºC at 140ºW. Evaporation at 15ºC is 17hPa that would pro-rate to about 2.2$mmday^{-1}$. The cold Humboldt Current flows alongside Atacama Desert in Chile and Peru, one of the driest deserts in the world. Precipitation is negligible with only pre-dawn dew as evidence of evaporation and condensation.

Humboldt Current is visible in the top millimeter ocean temperatures in the 2001 global satellite image (Figure 21). The ~19,000km track of the water mass from Chile to the mid-Pacific takes about 4.5yr. From there the Heyerdahl gyre moves westwards into the complex western boundary currents where cold older (age <25y) NH waters are advected in an equatorward low latitude western boundary current [65]. This southbound western boundary current is a consequence of the restrictive 50m deep Bering Strait. There is no comparable current in the North Atlantic that has deep access to the Arctic Ocean. Asymmetric SH warming explains why 21st century ENSO events are weaker and less predictable than in 20th century [66]. Indeed, human induced climate change forcing (AGW) now dominates all natural and solar cycles including the well-known decadal sunspot cycles driving major ocean indices including ENSO, ADO, PDO [67].

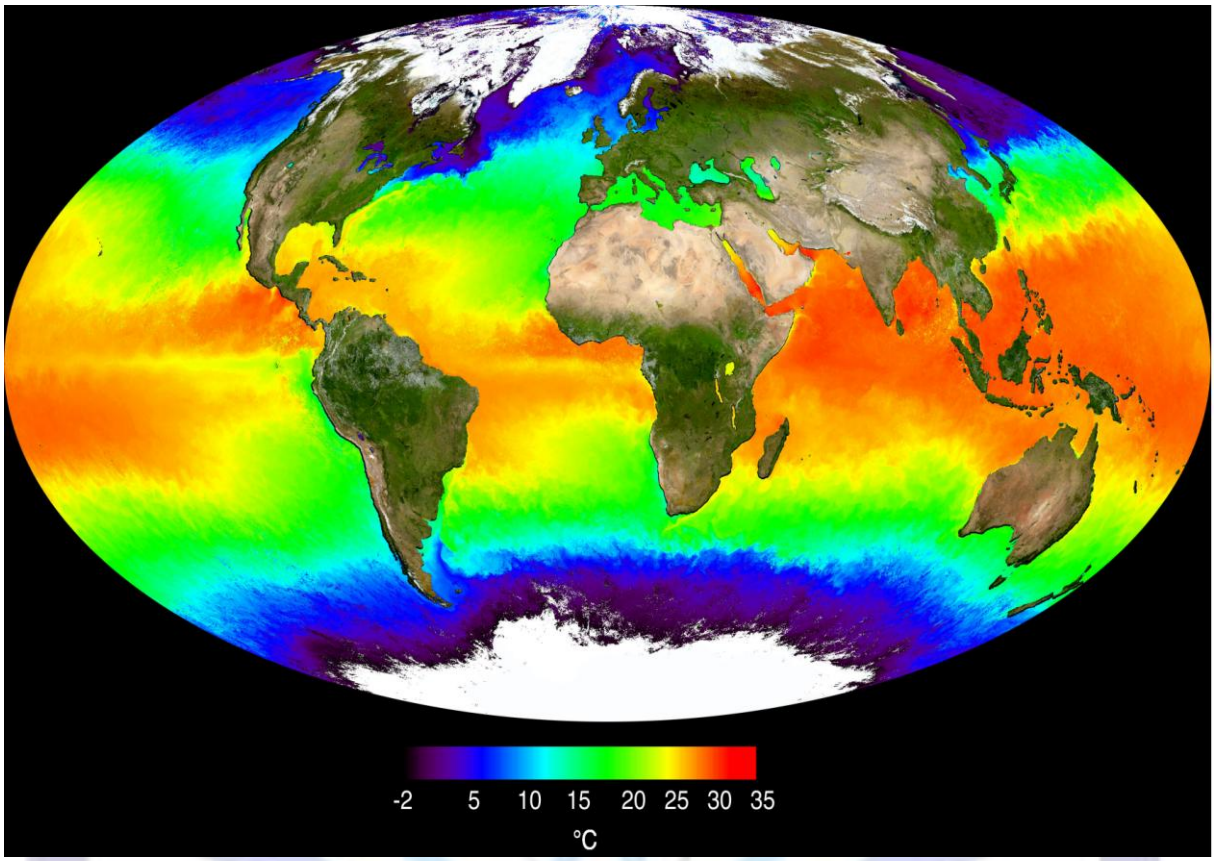

Figure 21 Satellite top millimeter sea surface temperature May 2001, courtesy Jacques Descloitres, MODIS Land Rapid Response Team, NASA/GSFC

We showed that rapid warming post 1986 of ~1ºC in 20 years coincided with a sharp decline in sunspot irradiation [1]. This suggests that all decadal ocean indices will continue to weaken as the temperature differences decline through continued ocean warming.

However, the three oceans have quite different northern boundaries and therefore circulation systems. Weak Atlantic equatorial upwelling is visible at ~25ºC (Figure 21). SH Atlantic northbound Benguela current flow at ~15ºC along the eastern boundary is similar to the Humboldt but does not reach the equator. By contrast, the NH Indian Ocean is completely landlocked with temperatures ~30ºC. This suggests that the Indian Ocean has reduced heat sequestration with enhanced evaporation at salinity ~36.4‰. This would support the observed salinity increase of ~0.6 in subtropical (~33ºS) Indian Ocean water from 1965-2002 [68].

The SH Indian Ocean shows northbound flow ~15ºC along the southwestern Australian coast but soon warms in the tropics without a cold surface current reaching the surface at equator. The SH Indian Ocean Agulhas southbound western boundary current from 27ºS is narrow swift and strong. NH Indian Ocean is warmer than the other oceans and includes

part of the Indo-Pacific warm pool. This suggests flow through Torres Strait and Arafura Sea. This is the source water region for the Pacific EUC thus connecting the SH and NH estuarine surface circulations. Thus, divergent equatorial near-surface ocean estuarine circulation forms a global circulation system with restrictions in shallow straits.

3.2 Increased precipitation, flooding and sealevel change

Since evaporation increases at a rate of ~7%ºC^{-1} under Clausius-Clapeyron we expect precipitation derived from high evaporation regions to increase by ~2-3%ºC^{-1}. Precipitation however, is not uniformly distributed. Walker zonal and meridional Hadley cells carry the enhanced evaporation from the central tropical Pacific. These cells are also an important ocean surface circulation mechanism through heat transport across the Panama Isthmus [17]. Precipitation strengthens estuarine stratification stability. Moreover, increased evaporation leads to a non-linear increase in atmospheric content of the greenhouse gas water vapor. This suggests a positive feedback effect. Surface salinity has decreased ~1.5‰ and temperatures increased ~1.5ºC west of ~180ºW over the past 50 years [69]. This is consistent with increased precipitation through the zonal Walker convection and strengthened estuarine stratification. A very strong La Niña has been reported consistent with increased equatorial warming [70]. Our data suggest weaker ENSO cycles and possibly permanent La Niña conditions are likely to ensue.

Increased precipitation has already been recorded in the southern hemisphere. From early 2010 to late 2011 record rainfall on land over Australia, Southeast Asia, and South America resulted and flooding and a global fall in sea level by 7mm [71]. Previously sealevel had been rising by ~3mm per year.

3.3 Tropical storms and heat dissipation

Higher surface temperatures suggest higher storm frequencies that act as a partial safety valve for extracting excess ocean heat. Tropical cyclone heat potential is determined from sea-surface-to-26ºC isotherm [72]. All thunderstorms have classic anvil tops of cirrus ice crystals (Figure 19). Strong downdrafts bring cold precipitation to the surface. Cold water with its 3000x higher heat capacity cools the surface in tropical fresh warm pools. This may temporarily cut off the storm heat source. The effect is likely to be relatively small because of the enormous heat capacity of the ocean surface layer. The upper 2m contains more heat than the entire atmosphere above [12].

Upwelling of subsurface colder subsurface (>3m) water requires sustained winds ~10ms^{-1} over a couple of days. Analysis of 40yr of hurricane data shows the critical factor is cyclone speed-over-ground (SOG) [73]. SOG >4.5ms^{-1} leaves too short a time to cool the surface. For an average storm over ~640km this is about 40hr or about 2d. These storms may go on to grow to Category 5 hurricanes defined as having windspeeds >50ms^{-1}. However, with SOG <4.5ms^{-1} the surface cools from upwelling and precipitation so the cyclone is downgraded. Thus fast moving storms grow larger because they are not sustained long enough in one place to bring up cooling water from >2-3m below the surface. This is the classical ocean parameter that fetch and time are needed to build to maximum wave height.

The tropical storm cooling effect has already been reported from satellite observation of storm-track haline wakes [74]. The estuarine Orinoco-Amazon 29ºC plume in south Atlantic had a 105 km^2 wake with ~+1.5‰ salinity increase and ~3.5ºC cooling. This is enough to cool the storm source water below 26ºC and dissipate heat. At higher latitudes winter storms are reported to result in surface heat loss and deepening halocline [75]. This is not due to evaporative heat loss, but upwelled subsurface warmer, more saline water. With ~1800 storms raging at any one time these are important to the global heat balance. Ongoing ocean warming suggests storms will become more frequent and lead to a new higher equilibrium state. However, getting heat out of the ocean will become more difficult if there are more widespread freshwater barriers from enhanced precipitation and runoff.

Indeed, freshwater warm pools with temperatures ~32ºC in the western Pacific create record-breaking super-typhoons. Western Pacific container shipping companies such as Maersk already use two new higher levels to characterize super-typhoons above Hurricane Force 12 on the Beaufort scale. Super typhoons have sustained windspeeds in excess of

65ms^{-1}. The greatest recorded super typhoon Haiyan in the Philippines in November 2013 had windspeeds in excess of 86 ms^{-1}. Our analysis suggests similar processes are likely in the tropical north Atlantic from salinity dominant surface processes at >36‰ and temperatures >28º. Indeed there were simultaneous hurricanes off the east and west Mexican coasts in 2013.

3.4 Future research through multidisciplinary global adaptive management

Our findings need verification through further analysis and experiment along other 3m meridional transects. Indeed, there are likely more research vessel data with 3m thermosalinograph timeseries that, so long as measurements are close to the seawater intake, and to oceanographic standards would be ideal for further research [8, 9]. Similar data from weatherships defined detailed processes in the top 100m from meteorological and oceanographic soundings along with nutrient sampling and plankton tows [76]. Plankton tows cannot be done from satellites. Indeed plankton studies first revealed the existence of Lagrangian ocean surface jet streams [20, 1]. Weatherships were discontinued in the 1970s [77]. Modern moored buoys and satellites do not have comparable timeseries in the crucial upper 100m let alone the crucial top 3m. Indeed we pointed out that cessation of hourly and daily monitoring of crucial top of the ocean processes coincided with the onset of rapid ocean warming [78]. Loss of monitoring led to missing the significance of hypersaline water in the Irish and North Seas from the mid-1980s. The peak in 1992-4 of water >36‰ was not seen in corresponding samples in the North Sea (Cornelius de Jager, personal correspondence). However, a 140yr record of Rhine river water and runoff shows sharply rising trend in volumes since the mid 1980s [80]. A similar marked increased freshwater input from European rivers into the Arctic Ocean estuary since the millennium is well known [81]. This supports our suggestion that continued ocean warming will see a thickening of the freshwater ocean layer from higher precipitation and runoff. The hypersaline water recorded at the Isle of Man is likely to have been a unique appearance of hypersaline water at the surface.

3.5 Scientific method depends on field verification not numerical models

We reported that numerical model and statistical studies were substituted for crucial daily and hourly monitoring with the result that the great climate changes from the 1976-1986 were completely missed [1, 78]. Our findings run contrary to accepted beliefs and are hard to present in the peer-review process [1]. Nonetheless evaporation through Clausius-Clapeyron mechanism is well-established meteorological principle. Emeritus Professor of Meteorology, Alistair Fraser, highlights the difficulty in overcoming established but wrong and unverified concepts on his Bad Science website (http://www.ems.psu.edu/~fraser/BadScience.html). He quotes Cardinal Wolsey (1471-1530), “Be very, very careful what you put into that head, because you will never, ever get it out”. For example, he showed the belief that raindrops are shaped like teardrops is still widely held despite experimental evidence to the contrary that we reported as long ago as 1964 [82]. He specifically highlights the ’myth’ that evaporation depends on relative humidity and windspeed. The website confirms from the Clausius-Clapeyron relationship that evaporation depends solely on temperature (http://fermi.jhuapl.edu/people/babin/vapor/index.html). Charles Keeling’s diligent monitoring of carbon dioxide concentrations is now well established. However, it is still considered controversial in non-science based discussions. Funding for essential long-term monitoring is hard to sustain as Keeling reported in his career review paper [83]. Keeling’s paper should be required reading for those conducting innovative research dependent on geophysical timeseries.

Near-surface ocean research requires re-evaluation through targeted multidisciplinary field verification. Much of the information on the Arctic boundary layer reported earlier derived from targeted multidisciplinary adaptively managed ecological process study in relation to offshore fossil fuel impact assessment [84]. This management system works most effectively when targeted from outset and confined to specific regions. The same process applied to national fisheries management was highly effective but far less so for international fishery management [85].

3.6 Sign of catastrophic impacts of global warming

We noted that tundra and sub sea anhydrous methane is already being released from global warming [1,78]. Continued warming from greenhouse gases is inevitable for the next century. Efforts now need to concentrate on reducing greenhouse gas concentrations as a matter of urgency. Removing ocean heat through geothermal and ocean heat exchangers is something that can be accomplished on a local scale but with potential global impact. Energy efficiency may be accomplished through individual carbon-neutral buildings. Coupled with tidal, hydroelectric, solar and wind technologies it may be possible to mitigate the worst effects global warming.

4 CONCLUSIONS

We conclude that ocean physics of the almost unstudied top 2m of ocean can explain all observed global warming over the past 250 years. These processes are summarized in our Figure 20. Observed asymmetries are a consequence of fundamental classical physics. The first hurdle is for full scientific verification of our results from other fieldwork according to the scientific method. However, the underlying classical physics principles are already well established. We hope this work will stimulate monitoring and mitigation research in order to avoid catastrophic unpredictable consequences of human induced impacts on Earth's interconnected physical, chemical, and biological systems.

ACKNOWLEDGMENTS

We are grateful to Don Williamson and Curtis Ebbesmeyer for helpful comments on a draft of this paper, to William Crawford for clarification of Line P surface temperature shift, and to Donald A Thompson for Gulf of California fisheries and tidal data, and to Cornelius de Jager to redraw his 400yr sunspot/global warming data and discussion of the ocean surface processes. Nina Matthews' assistance and proof reading are gratefully acknowledged. JBRM acknowledges the Sea Education Association (www.sea.org) for scholarship awards and for granting access to data from the SRV Robert C. Seamans May–June 2008 and Isle of Man government support. Research reported here was self-funded.

REFERENCES

[1] Matthews, J. B. and Matthews, J. B. R.: Possible signals of poleward surface ocean heat transport, of Arctic basal ice melt, and of the twentieth century solar maximum in the 1904–2012 Isle of Man daily timeseries, Ocean Sci. Discuss., 11, 47–122, doi:10.5194/osd-11-47-2014, 2014.

[2] Levitus, S., Antonov, J. I., Boyer, T. P., Baranova, O. K., Garcia, H. E., Locarnini, R. A., Mishonov, A. V., Reagan, J. R., Seidov, D., Yarosh, E. S. and Zweng, M. M.: World ocean heat content and thermosteric sea level change (0-2000 m), 1955-2010, Geophys. Res. Lett., 39, L10603, doi:10.1029/2012GL051106, 2012.

[3] Rohde, R., Muller, R. A., Jacobsen, R., Muller, E., Perlmutter, S., Rosenfeld, A., Wurtele, J., Groom, D. and Wickham, C.: A new estimate of the average earth surface land temperature spanning 1753 to 2011, Geoinfor Geostat: An Overview, 1, 1, 7pp, doi: 10.4172/gigs.1000101, 2012.

[4] Katsman, C. A. and van Oldenborgh, G. J.: Correction to "Tracing the upper ocean's 'missing heat'", Geophys. Res. Lett., 38, L20602, doi:10.1029/2011GL049834, 2011.

[5] Hobbs, W. R. and Willis, J. K.: Detection of an observed 135 year ocean temperature change from limited data, Geophys. Res. Lett., 40, 2252-2258, doi:10.1002/grl.50370, 2013.

[6] Roemmich, D., Gould, W. J. and Gilson, J.: 135 years of global ocean warming between the Challenger expedition and the Argo Programme, Nature Clim. Change, 2, 425-428, doi:10.1038/nclimate1461, 2012. Sannella, M. J. 1994 Constraint Satisfaction and Debugging for Interactive User Interfaces. Doctoral Thesis. UMI Order Number: UMI Order No. GAX95-09398., University of Washington.

[7] Douglass, D. H. and Knox, R. S.: Ocean heat content and Earth's radiation imbalance. II. Relation to climate shifts, Phys. Lett. A, 376, 1226-1229, doi:10.1016/j.physleta.2012.02.027, 2012.

[8] Matthews, J. B. R.: Comparing historical and modern methods of sea surface temperature measurement - Part 1: Review of methods, field comparisons and dataset adjustments, Ocean Sci., 9, 683-694, doi:10.5194/os-9-683-2013, 2013.

[9] Matthews, J. B. R. and Matthews, J. B.: Comparing historical and modern methods of sea surface temperature measurement - Part 2: Field comparison in the central tropical Pacific, Ocean Sci., 9, 695-711, doi:10.5194/os-9-695-2013, 2013.

[10] Emery, W. J. and Thomson, R. E.: Data Analysis Methods in Physical Oceanography, Elsevier, 2001.

[11] Matthews, J. B. R.: Seasonal variability of sea surface carbonate chemistry and temperature, PhD Thesis, available at: http://dspace.library.uvic.ca:8080/handle/1828/5104, 2013.

[12] Soloviev, A. and Lukas, R.: The Near-Surface Layer of the Ocean: Structure, Dynamics and Applications, Springer, Dordrecht, The Netherlands, 2006.

[13] Crawford, W., Galbraith, J. and Bolingbroke, N.: Line P ocean temperature and salinity, 1956–2005, Prog. Oceanogr., 75, 161-178, doi:10.1016/j.pocean.2007.08.017, 2007.

[14] Hansen, D. V. and Rattray Jr., M.: New Dimensions in Estuary Classification, Limnol. Oceanogr., 11, 319-326, 1966.

[15] Tully, J. P. and Barber, F. G.: An Estuarine Analogy in the Sub-Arctic Pacific Ocean, J. Fish. Res. Bd. Can., 17, 91-112, doi:10.1139/f60-007, 1960.

[16] Stigebrandt, A.: The North Pacific: A Global-Scale Estuary, J. Phys. Oceanogr., 14, 464-470, doi:10.1175/1520-0485(1984)014<0464:TNPAGS>2.0.CO;2, 1984.

[17] Carmack, E. C.: The alpha/beta ocean distinction: A perspective on freshwater fluxes, convection, nutrients and productivity in high-latitude seas, Deep-Sea Res. Pt. II; Effects of Climate Variability on Sub-Arctic Marine Ecosystems - A GLOBEC Symposium, 54, 2578-2598, doi:10.1016/j.dsr2.2007.08.018, 2007.

[18] Peacock, T. and Haller, G.: Lagrangian coherent structures: The hidden skeleton of fluid flows, Physics Today, 66(2), 41-47, doi: 10.1063/PT.3.1886, 2013.

[19] Lin, J., Brunner, D., Gerbig, C., Stohl, A., Luhar, A. and Webley, P. (Eds.): Lagrangian Modelling of the Atmosphere, Geoph. Monog. Series Vol. 200, AGU, Washington, DC, USA, 2013.

[20] Williamson, D. I.: Planktonic evidence for irregular flow through the Irish Sea and North Channel in the autumn of 1954, J. Mar Biol. Assoc. UK., 35, 461-466 461, 1956.

[21] Ebbesmeyer, C. and Scigliano, E.: Flotsametrics and the floating world, Harper Collins Pub. Co., ISBN 978-0-06-155841-2, 2009.

[22] Pugh, D. T.: Tides, surges and mean sea-level: a handbook for engineers and scientists, Wiley, Chichester, UK, 1987.

[23] Matthews, J. B.: Observations of surface and bottom currents in the Beaufort Sea near Prudhoe Bay, Alaska, J. Geophys. Res.-Oceans, 86, 6653-6660, doi:10.1029/JC086iC07p06653, 1981.

[24] Ingraham Jr., J.: Getting to know OSCURS, REFMS's Ocean Surface Current Simulator, Status of Stocks and Multispecies, Quarterly Report, Alaska Fisheries Science Center, June 1997, http://www.afsc.noaa.gov/REFM/docs/oscurs/get_to_know.htm, 1997.

[25] Dat, C. G., Leblond, P. H., Thomson, K. A., and Ingraham Jr, W. J.: Computer simulations of homeward-migrating Fraser River sockeye salmon: is compass orientation a sufficient direction-finding mechanism in the north-east Pacific Ocean?, Fish Oceanogr, 4(3), 209-216, doi:10.1111/j.1365-2419.1995.tb00144.x, 1995.

[26] Ebbesmeyer, C.C., Belkin, I. M., Drost, H. E., Zimmermann, S., and Carmack, E. C.: Wall across the Atlantic: Drift bottles released by students confirm that the Gulf Stream prevents subarctic surface drifters from escaping south, Oceanography, 24(1), 172–174, doi: 10.5670/oceanog.2011.15, 2011.

[27] Lavender-Law, K., Morét-Ferguson, S., Maximenko, N. A., Proskurowski, G., Peacock, E. E., Hafner, J., and Reddy, C. M.: Plastic Accumulation in the North Atlantic Subtropical Gyre, Science, 329(5996), 1185-1188, doi:10.1126/science.1192321, 2010.

[28] Maximenko, N., Hafner, J. and Niiler, P.: Pathways of marine debris derived from trajectories of Lagrangian drifters, Mar. Pollut. Bull., 65, 51-62, doi:10.1016/j.marpolbul.2011.04.016, 2012.

[29] Van Sebille, E., England, M. H., and Froyland, G.: Origin, dynamics and evolution of ocean garbage patches from observed surface drifters, Environ Res Lett,, 7(4), doi:10.1088/1748-9326/7/4/044040, 2012.

[30] Lumpkin, R., and Johnson, G. C.: Global ocean surface velocities from drifters: Mean, variance, El Nino–Southern Oscillation response, and seasonal cycle, J. Geophys. Res. Oceans, 118, 2992–3006, doi:10.1002/jgrc.20210, 2013.

[31] Kara, A. B., Wallcraft, A. J., Metzger, E. J., Hurlburt, H. E. and Fairall, C. W.: Wind Stress Drag Coefficient over the Global Ocean, J. Climate, 20, 5856-5864, doi:10.1175/2007JCLI1825.1, 2007.

[32] Williams, R. G. and Follows, M. J.: Ocean Dynamics and the Carbon Cycle, Cambridge University Press, Cambridge, UK, 2011.

[33] Gill, A.: Atmosphere-Ocean Dynamics, Academic Press, New York, NY, USA, 1982.

[34] Lukas, R. and Firing, E.: The geostrophic balance of the Pacific Equatorial Undercurrent, Deep-Sea Res., 31, 61-66, doi:10.1016/0198-0149(84)90072-4, 1984.

[35] Grenier, M., Cravatte, S., Blanke, B., Menkes, C., Koch-Larrouy, A., Durand, F., Melet, A. and Jeandel, C.: From the western boundary currents to the Pacific Equatorial Undercurrent: Modeled pathways and water mass evolutions, J. Geophys. Res.-Oceans, 116, C12044, doi:10.1029/2011JC007477, 2011.

[36] Goodman, P. J., Hazeleger, W., de Vries, P. and Cane, M.: Pathways into the Pacific Equatorial Undercurrent: A Trajectory Analysis, J. Phys. Oceanogr., 35, 2134-2151, doi:10.1175/JPO2825.1, 2005.

[37] Johnson, G. C., Sloyan, B. M., Kessler, W. S. and McTaggart, K. E.: Direct measurements of upper ocean currents and water properties across the tropical Pacific during the 1990s, Prog. Oceanogr., 52, 31-61, doi:10.1016/S0079-6611(02)00021-6, 2002.

[38] Cronin, M. F. and McPhaden, M. J.: Barrier layer formation during westerly wind bursts, J. Geophys. Res. 107(C12), 802, doi: 10.1029/2001JC001171 , 2002.

[39] Cravatte, S., Delcroix, T., Zhang, D., McPhaden, M. and Leloup, J.: Observed freshening and warming of the western Pacific Warm Pool, Clim. Dyn., 33, 565-589, doi:10.1007/s00382-009-0526-7, 2009.

[40] Alory, G., Maes, C., Delcroix, T., Reul, N. and Illig, S.: Seasonal dynamics of sea surface salinity off Panama: The far Eastern Pacific Fresh Pool, J. Geophys. Res.-Oceans, 117, C4, doi:10.1029/2011JC007802, 2012.

[41] Cronin, M. F. and Kessler, W. S.: Near-Surface Shear Flow in the Tropical Pacific Cold Tongue Front, J. Phys. Oceanogr., 39, 1200-1215, doi:10.1175/2008JPO4064.1, 2009.

[42] Johnson, G. C., McPhaden, M. J. and Firing, E.: Equatorial Pacific Ocean Horizontal Velocity, Divergence, and Upwelling, J. Phys. Oceanogr., 31, 839-849, doi:10.1175/1520-0485(2001)031<0839:EPOHVD>2.0.CO;2, 2001.

[43] Weisberg, R. H. and Qiao, L.: Equatorial Upwelling in the Central Pacific Estimated from Moored Velocity Profilers, J. Phys. Oceanogr., 30, 105-124, doi:10.1175/1520-0485(2000)030<0105:EUITCP>2.0.CO;2, 2000.

[44] Reid, J. L.: Some Advances and Retreats in the Study of Ocean Circulation since 1935, in: Physical Oceanography, Jochum, M. and Murtugudde, R. (Eds.), Springer, New York, NY, USA, 165-179, doi:10.1007/0-387-33152-2_11, 2006.

[45] Johnston, T. M. S., Rudnick, D. L. and Pallàs-Sanz, E.: Elevated mixing at a front, J. Geophys. Res.-Oceans, 116, doi:10.1029/2 011JC007192, 2011.

[46] Simpson, H. J., Herczeg, A. L. and Meyer, W. S.: Stable isotope ratios in irrigation water can estimate rice crop evaporation, Geophys. Res. Lett., 19, 377-380, doi:10.1029/91GL02952, 1992.

[47] Perez, R. C., Cronin, M. F. and Kessler, W. S.: Tropical Cells and a Secondary Circulation near the Northern Front of the Equatorial Pacific Cold Tongue, J. Phys. Oceanogr., 40, 2091-2106, doi:10.1175/2010JPO4366.1, 2010.

[48] Andutta, F. P., Ridd, P. V. and Wolanski, E.: Dynamics of hypersaline coastal waters in the Great Barrier Reef, Estuar. Coast. Shelf Sci., 94, 299-305, doi:10.1016/j.ecss.2011.06.009, 2011.

[49] Cronin, M. F., and McPhaden, M. J.: Upper ocean salinity balance in the western equatorial Pacific, J. Geophys. Res. Oceans, 103(C12), 27567-27587, 1998.

[50] Sumner, D. M. and Belaineh, G.: Evaporation, precipitation, and associated salinity changes at a humid, subtropical estuary, Estuaries, 28, 844-855, doi:10.1007/BF02696014, 2005.

[51] Liu, W. T., Katsaros, K. B. and Businger, J. A.: Bulk Parameterization of Air-Sea Exchanges of Heat and Water Vapor Including the Molecular Constraints at the Interface, J. Atmos. Sci., 36, 1722-1735, doi:10.1175/1520-0469(1979)036<1722:BPOASE>2.0.CO;2, 1979.

[52] Smith, S. D.: Coefficients for sea surface wind stress, heat flux, and wind profiles as a function of wind speed and temperature, J. Geophys. Res.-Oceans, 93, 15467-15472, doi:10.1029/JC093iC12p15467, 1988.

[53] Woods, G. S., Ruxton, A., Huddlestone-Holmes, C. and Gigan, G.: High-Capacity, Long-Range, Over Ocean Microwave Link Using the Evaporation Duct, IEEE J. Oceanic Eng., 34, 323-330, doi:10.1109/JOE.2009.2020851, 2009.

[54] Levitus, S., Antonov, J. I., Boyer, T. P. and Stephens, C.: Warming of the World Ocean, Science, 287, 2225-2229, doi:10.1126/science.287.5461.2225, 2000.

[55] Bray, N. A.: Water mass formation in the Gulf of California, J. Geophys. Res.-Oceans, 93, 9223-9240, doi:10.1029/JC093iC08p09223, 1988.

[56] Castro, R., Lavín, M. F. and Ripa, P.: Seasonal heat balance in the Gulf of California, J. Geophys. Res.-Oceans, 99, 3249-3261, doi:10.1029/93JC02861, 1994.

[57] Karnauskas, K. B., Johnson, G. C. and Murtugudde, R.: An Equatorial Ocean Bottleneck in Global Climate Models, J. Climate, 25, 343-349, doi:10.1175/JCLI-D-11-00059.1, 2012.

[58] Cubukcu, N. and Krishnamurti, T. N.: Low-Frequency Controls on the Thresholds of Sea Surface Temperature over the Western Tropical Pacific, J. Climate, 15, 1626-1642, doi:10.1175/1520-0442(2002)015<1626:LFCOTT>2.0.CO;2, 2002.

[59] Wijesekera, H. W., Rudnick, D. L., Paulson, C. A., Pierce, S. D., Pegau, W. S., Mickett, J. and Gregg, M. C.: Upper ocean heat and freshwater budgets in the eastern Pacific warm pool, J. Geophys. Res.-Oceans, 110, doi:10.1029/2004JC002511, 2005.

[60] Carton, J. A. and Santorelli, A.: Global Decadal Upper-Ocean Heat Content as Viewed in Nine Analyses, J. Climate, 21, 6015-6035, doi:10.1175/2008JCLI2489.1, 2008.

[61] von Schuckmann, K. and Le Traon, P.-Y.: How well can we derive Global Ocean Indicators from Argo data?, Ocean Sci., 7, 783-791, doi:10.5194/os-7-783-2011, 2011.

[62] Moreira-Turcq, P. F.: Impact of a low salinity year on the metabolism of a hypersaline coastal lagoon (Brazil), Hydrobiologia, 429, 133-140, doi:10.1023/A:1004037624787, 2000.

[63] Trenberth, K. E.: El Niño Southern Oscillation (ENSO), in: Encyclopedia of Ocean Sciences (Second Edition), Steele, J. H., Turekian, K. K. and Thorpe, S. A. (Eds.), Elsevier, 228-240, 2008.

[64] McPhaden, M. J., Busalacchi, A. J. and Anderson, D. L. T.: A TOGA Retrospective, Oceanography, 23, 86-103, doi:10.5670/oceanog.2010.26, 2010.

[65] Fine, R. A., Lukas, R., Bingham, F. M., Warner, M. J. and Gammon, R. H.: The western equatorial Pacific: A water mass crossroads, J. Geophys. Res.-Oceans, 99, 25063-25080, doi:10.1029/94JC02277, 1994.

[66] McPhaden, M. J.: Evolution of the 2006–2007 El Niño: the role of intraseasonal to interannual time scale dynamics, Adv. Geosci., 14, 219-230, doi:10.5194/adgeo-14-219-2008, 2008.

[67] Pierce, D.W., Gleckler, P. J., Barnett, T. P., Santer, B. D., and Durack, P. J. : The fingerprint of human induced changes in the ocean's salinity and temperature fields, Geophys. Res. Lett., 39, L21704, doi:10.1029/2012GL053389, 2012.

[68] Bryden, H. L., McDonagh, E. L. and King, B. A.: Changes in Ocean Water Mass Properties: Oscillations or Trends?, Science, 300, 2086-2088, doi:10.1126/science.1083980, 2003.

[69] Durack, P. J. and Wijffels, S. E.: Fifty-Year Trends in Global Ocean Salinities and Their Relationship to Broad-Scale Warming, J. Climate, 23, 4342-4362, doi:10.1175/2010JCLI3377.1, 2010.

[70] Boening, C., Willis, J. K., Landerer, F. W., Nerem, R. S. and Fasullo, J.: The 2011 La Niña: So strong, the oceans fell, Geophys. Res. Lett., 39, doi:10.1029/2012GL053055, 2012.

[71] Fasullo, J.: Australia's record rains lowered sea level, Nature, 500(7464), 504, doi:10.1038/500504a, 2013.

[72] Wada, A. and Chan, J. C. L.: Relationship between typhoon activity and upper ocean heat content, Geophys. Res. Lett., 35, doi:10.1029/2008GL035129, 2008.

[73] Mei, W., Pasquero, C. and Primeau, F.: The effect of translation speed upon the intensity of tropical cyclones over the tropical ocean, Geophys. Res. Lett., 39, L07801, doi:10.1029/2011GL050765, 2012.

[74] Grodsky, S. A., Reul, N., Lagerloef, G., Reverdin, G., Carton, J. A., Chapron, B., Quilfen, Y., Kudryavtsev, V. N. and Kao, H.-Y.: Haline hurricane wake in the Amazon/Orinoco plume: AQUARIUS/SACD and SMOS observations, Geophys. Res. Lett., 39, doi:10.1029/2012GL053335, 2012.

[75] Kang, Y. J., Noh, Y. and Yeh, S.-W.: Processes that influence the mixed layer deepening during winter in the North Pacific, J. Geophys. Res.-Oceans, 115, doi:10.1029/2009JC005833, 2010.

[76] Pingree, R. D. and Plevin, J.: A description of the upper 100 m at Ocean Weather Station Juliett (52°30'N, 20°00'W), Deep-Sea Res., 19, 21-34, doi:10.1016/0011-7471(72)90070-8, 1972.

[77] Downes, C. R.: History of the British Ocean Weather Ships, Marine Observer, 47, 179-186, 1977.

[78] Matthews, J. B. and Matthews, J. B. R.: Isle of Man daily surface timeseries 1904-2012, Arctic basal ice melt, sunspots, and ocean warming, Ocean Sci., In Press, doi:10.5194/osd-11-47-2014, 2014.

[79] De Jager, C., Duhau, S., and van Geel, B.: Quantifying and specifying the solar influence on terrestrial surface temperature, J. Atmos. Sol-Terr. Phy., 72. 926–937, doi:10.1016/j.jastp.2010.04.011, doi:10.1016/j.jastp.2010.04.011, 2010.

[80] van Aken, H. M.: Variability of the salinity in the western Wadden Sea on tidal to centennial time scales, Journal of Sea Research, 59, 121–132, 2008.

[81] McClelland, J. W., Holmes, R. M., Dunton, K. H. and Macdonald, R. W.: The Arctic Ocean Estuary, Estuar. Coast., 35, 353-368, doi:10.1007/s12237-010-9357-3, 2012.

[82] Matthews, J. B., and Mason, B. J.: Electrification produced by the rupture of large water drops in an electric field, Q J Roy Meteor Soc, 90(385), 275-286, doi: 10.1002/qj.49709038506, 1964.

[83] Keeling, C. D.: Rewards and Penalties of Monitoring the Earth, Ann Rev Energ Env, 23(1), 25-82, doi: 10.1146/annurev.energy.23.1.25, 1998.

[84] Matthews, J. B.: Modelling and Verification of Circulation in an Arctic Barrier Island Lagoon System - An Ecosystem Process Study, in: Mathematical Modelling of Estuarine Physics, Sündermann, J. and Holz, K.-P. (Eds.), Springer-Verlag, New York, NY, USA, 220-231, doi:10.1029/LN001p0220, 1978.

[85] Walters, C. J. and Martell, S. J. D.: Fisheries Ecology and Management, Princeton University Press, Princeton, NJ, USA, 2004.

META DATA BIO STATEMENT

J. B. Robin Matthews

Post Doctoral Fellow, Dept Physics and Physical Oceanography, Memorial University of Newfoundland, St Johns, NL Canada 2014. PhD School of Earth and Ocean Sciences, University of Victoria, Victoria, BC Canada Supervisor Andrew Weaver, Thesis: Seasonal variability of sea surface carbonate chemistry and temperature, http://dspace.library.uvic.ca:8080/handle/1828/5104, 2013. BSc (First Class), Geophysical Sciences, University of East Anglia, UK, 2009, Final Year Thesis Supervisor Phil Jones, Climate Research Unit. Dean‟s and President‟s Award, Sea Education Association, SEA Semester Class 217- SSV Robert C Seamans, Woods Hole MA, USA 2008. School of Earth and Ocean Sciences, University of British Columbia, Vancouver, Canada 2007-8. BBC Blue Peter Award and Reporter BBC TV Newsround report on Manx Basking Sharks.